Estimating Key Components for Physics- Based Vision: Reflectance Estimation with the Presence of Inter-Reflection and Camera Sensitivity Recovery

物理法則に基づくビジョン研究の基礎要素の推定：相互反射を考慮した物体表面反射率推定およびカメラ感度関数推定

BY

Hongxun Zhao 趙 宏勛

A Master Dissertation

Submitted to the Graduate School of
the University of Tokyo

in Partial Fulfillment of the Requirements
for the Degree of
Master of Information Science and Technology

AUGUST 2009

Thesis Supervisor: Katsushi IKEUCHI　池内克史

ABSTRACT

Physics-based vision is one field of the computer vision. By using physics-based vision methods, we could accurately estimate the geometrical and optical properties of real object from images. Physics-based vision is concerned with the physical relationship between an imaging sensor and the external world. The physical phenomenon that mediates this relationship is light. Consequently, two key components of physics-based vision are reflection models and sensor models.

This thesis investigates these two key components, the reflection models and sensor models. Specifically, for reflection models we proposed a practical method to estimate the reflectance properties of outdoor diffuse object with the presence of inter-reflection. For sensor models, we investigated the characteristics of spectral sensitivity and proposed a robust method to estimate spectral sensitivity of digital cameras by using basis functions.

To create a realistic model of a real world object by computer vision and graphics techniques has attracted interest from a wide range of research fields and industries in recent years. Reflectance properties of the object are necessary to simulate the accurate appearance of an object. However, wrong reflectance parameters are estimated, when inter-reflection exists. Inter-reflections are negligible for convex objects, while it is not for concave objects. We addressed a method to estimate reflectance properties of an outdoor diffuse object with the presence of inter-reflection. This problem is solved by assuming that the object surface consists of hundreds of small facets. The inter-reflection effect on one facet is calculated as the sum of incoming light energy from all other facets. Experimental evaluation on both simulation and real outdoor object shows the improvement achieved by the proposed method.

Spectral sensitivity of digital cameras plays an important role for many computer vision applications, such as demosaicing, color correction and illuminant estimation algorithms. Spectral sensitivity is also an essential factor for most color constancy methods. However, previous work does not provide reliable estimation for spectral sensitivity. We investigated the characteristics of spectral sensitivity by extracting the basis functions of them by using SVD (Singular Value Decomposition); sensitivity of different cameras have been measured, also collected from the literature. We compared the extracted basis functions with another three different mathematical basis functions: polynomial basis functions, Fourier basis functions and radial basis functions (RBF), and obtained the optimum set. Experimental result shows the extracted basis functions are reliable and adequate to estimate the spectral sensitivity for an arbitrary digital

camera.

The main contributions of this thesis are that two key components of physics-based vision are investigated, reflectance estimation with the presence of inter-reflection and camera sensitivity recovery. It can be summarized by the two following points: First, reflectance of an outdoor diffuse object with the presence of inter-reflection is accurately estimated by assuming the object surface consists of hundreds of small facets, inter-reflection effect on one facet is calculated as the incoming light energy from all the other facets. Second, characteristics of spectral sensitivity are investigated, and basis functions extracted from database are used for estimating the spectral sensitivity of an arbitrary digital camera.

Acknowledgements

First and foremost, I would like to acknowledge and extend my heartfelt gratitude to my thesis supervisor, Prof. Katsushi Ikeuchi, for his consideration and supervision. He encouraged and challenged me during every meeting, and gave me a lot of great ideas to solve the problem. His profound learning and down-to-earth attitude left a deep impression on me. I also would like to thank him for a great research environment provided in his laboratory.

My appreciation goes to Dr. Rei Kawakami of my direct senior associate. She is always patient with me and gave me significant advice to my research. I learned from her how to be a good researcher. I still remember she revising my paper line by line. She also made great efforts to make me adapt life in japan. I really appreciate the efforts she made for both my research and life.

Many thanks go to the people that I have been working with, the current and former members of the Computer Vision Laboratory at the University of Tokyo. Special thanks go to Dr. Robby T.Tan, who found time to direct me to overcome the difficulty and continue my research in the midst of all his activities, to Dr. Jun Takamatsu, who kindly helped me when i asked for the source code of one of his work and explained details to me, to Dr. Bo Zheng, who always helped me to solve the problem and concerned about my life. I would like to thank Tetsuya Kakuta, Tetsuro Morimoto, and Tomoaki Higo, for having interesting and fruitful discussions with me regarding the field of physics-based vision, to Bjoern Rennhak, Mawo Kamakura, Ulinta Ginting, Phongtharin Vinayavekhin, Jinge Wang, Sonoko Okura, and Boun Vinh Lu, for making my lab-time enjoyable. I am also indebted to Kiminori Hasegawa, Keiko Motoki, Yoshiko Matsuura, Kaoru Kikuchi, and Mikiko Yamaba, for help me going through the admission procedures and other procedures needed in my department.

Last but not least, I would like to pay my highest tribute to my family, my dear

mother and father. It was them that supported me during these years to make it possible to concentrate on my study and research. It was them that consoled me when i was upset and encouraged me to go ahead. I could not accomplish anything without their understanding and support. I dedicate this dissertation to my family.

August 2009
Hongxun Zhao

Contents

List of Figures

List of Tables

Chapter 1

Introduction

1.1 Background

Physics-based vision has attracted much attention in the field of computer vision since the concept has been addressed in the late 1980s. Much more accurate geometrical and optical information of objects could be acquired by physics-based vision methods. In physics-based vision, computer vision is modeled as process of physical phenomenon/optical phenomenon. By the definition of physics-based vision, it is concerned with the physical relationship between an imaging equipment and the real objects. Therefore, two key components of physics-based vision are reflection models and sensor models. Reflection models are the interaction of light with material objects through the physical process of reflection and transmission. Sensor models are the formation of sensor pixel intensities from the interaction of reflected light with lens optics and photo-optical electronics. These two key components are investigated and two novel methods are proposed. Specifically, for reflectance models we proposed a practical method for estimating reflectance of outdoor diffuse object with the presence of inter-reflection, for sensor models we proposed a robust method for estimating the spectral sensitivity of digital cameras by using basis functions.

Reflectance Estimation Computer vision and graphics techniques to create a realistic model of a real world object have attracted interest from a wide range of research fields and industries in recent years. To simulate the accurate appearance of an object, shape and optical information are necessary. Acquiring shape information has been facilitated

by the development of sensors and the progress of data processing algorithms, while estimating surface reflectance properties remains a challenge, especially for outdoor objects.

Several modeling methods with range sensors were proposed [6] [9]; however those methods created surface textures by simply blending images taken from multiple views. Meanwhile, physics-based reflectance estimation methods [10] [12], photometric stereo techniques [57] [58] [59], and image-based rendering techniques [14] have been proposed to create more physically correct object appearances. Physics-based reflectance estimation is based on physical reflection models [60] and estimates the parameters of the models by fitting the data to them. The methods have achieved highly accurate re-renderings, yet they need accurately calibrated illuminants and cameras. Photometric stereo is a method that captures images under three different lighting conditions and estimates the surface reflectance and the surface normal of the shape. It assumes a known distant point light source, and therefore it is unsuitable for outdoor conditions. Image-based rendering is a technique that samples appearances under a number of different lighting conditions, and re-renders the appearance by interpolating the images. Creating such a number of different illumination conditions is impractical for an outdoor environment, and so it is difficult to be applied to outdoor objects.

Debevec et al.[61] proposed a method to obtain the reflectance function with the position of light sources known. To extend this idea to outdoor scenes, Yu and Malik [30] measured the illumination of the scene by acquiring photographs of the sky and the surrounding environments. Most recently, Debevec [31] introduced a novel lighting measurement apparatus than can record the high dynamic range of both, sunlit and cloudy environments, using a set of specular and diffuse calibrated spheres. With the captured illumination, proposed method estimates spatially varying surface reflectance. Weiss [17] proposed a method to decompose an image into a reflectance image and an illumination image by assuming the change caused by reflectance remains constant in the image sequence, while the change caused by illumination varies depending on time. Therefore, by taking the median of derivative filter outputs of input images, the reflectance image can be estimated. Matsushita et al. [29] extended the idea so that it can handle non-Lambertian surfaces, and proposed an illumination normalization scheme utilizing the illumination eigen space and a shadow interpolation method based on shadow hulls.

Camera Sensitivity Recovery Spectral sensitivity plays an important role for many computer vision applications, such as demosaicing [18], color correction [19] and illumination estimation algorithms [20] [21]. CCD (Charge Coupled Device) sensors usually provide only single response at each pixel, demosaicing is used to recover response of R, G and B channels based on the spectral sensitivity for each pixel. Color correction is a method that correct the obtained image to compensate for the effects of the recording illumination. Illumination estimation is used for recovering the illumination by acquiring different images under different illumination environments. Spectral sensitivity is also an essential characteristic for color constancy methods. Captured appearance of object is different according to different illumination conditions. Color constancy method is used to remove the influence of light source and retrieve object surface color under standard illumination.

In computer vision and graphics research fields, a few methods that estimate the spectral sensitivity have been proposed. Vora et al. [32] measured the spectral sensitivity of two digital cameras: Kodak DCS-200 and Kodak DCS-420. In this paper, the target is illuminated by the monochrometer which could produce narrow-band illumination. While changing the wavelength, the images and spectra are simultaneously captured by camera and spectrometer, respectively. The spectral sensitivity is calculated by dividing the image intensity by the measured spectra. Hardeberg et al. proposed a method that estimates spectral sensitivity by inverting the system of linear equations obtained by image intensities and known spectral reflectance [24], while it has not been applied to real data because of the instability.

All these proposed methods of spectral sensitivity estimation require the image intensity as input. The image intensity is not linearly related to scene radiance because of the gamma function. In order to obtain the precise measurement of scene radiance to estimate the spectral sensitivity, the gamma function (also called as camera response function) must be estimated first. While less attention has been paid for estimating the spectral sensitivity, much attention has been paid for camera response estimation. Mann and Picard [55] proposed a method that assumes the response functions can be approximated by gamma correction functions. Debevec and Malik [56] estimate response functions with a non-parametric representation using a smoothness constraint. Takamatsu [22] proposed a method for estimating camera response functions by maximizing the image similarity measurement defined as the integral of the probabilistic intensity similarity.

1.1.1 Reflectance Estimation

With the acquisition of shape information of diffuse object, we need to estimate the absolute surface reflectance for recovering the appearance of the object under a novel illumination condition. Reflectance is the ratio of reflected light to the incident electromagnetic radiation, i.e., how much light a material will reflect regarding the incident light. This thesis defines the reflectance on each *RGB* channel; the maximum reflectance (no absorption) is (1.0, 1.0, 1.0) for (R, G, B). Figure 1.1 shows an example of surface reflectance. We can clearly see that the surface reflectance is the most essential component in terms of the object's surface property. However, we have to take the shape information into account.

For directly estimating surface reflectance properties, three components are necessary: the shape of a target object, the actual appearance of the object, and the illumination environment. Shape information and actual appearance can be obtained by range and image sensors, respectively. Two methods of recovering surface reflectance of outdoor objects measured the above three components. Yu et al. [30] the first who handled outdoor objects, took photographs of the sun and sky to measure their radiance distribution. As they used a normal camera, they included landmarks in each photograph so that they could use them to recover the camera pose later. Debevec et al. [31], the second and the latest to solve the outdoor problem, used a specific apparatus to measure the outside illumination. They used a mirrored sphere to image the sky and clouds, a shiny black sphere to indicate the position of the sun, and a diffuse grey sphere to indirectly measure the intensity of the sun. These methods need elaborate procedures and do not take the inter-reflection into account. Consequently, these methods could not be applied for outdoor objects which have concave parts. Because the inter-reflection effect is not negligible for the concave objects.

For concave objects or objects with concave parts, a point of object surface receives light from both light source and other points on the surface. The latter (reflection between points on object surface) is called as inter-reflection effect . Therefore, light rays that we observe for concave object is the result of reflections repeated between surface points infinitely. It is difficult to trace back those recursive reflections from the observation.

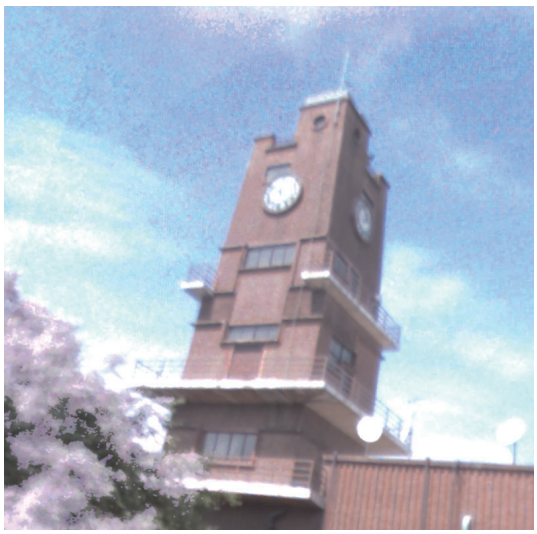

(a) Appearance.

(b) Shape and illumination.

(c) Surface reflectance.

Figure 1.1: The object's appearance is determined by its shape, surrounding illumination, and surface reflectance.

1.1.2 Camera Sensitivity Recovery

Spectral sensitivity of digital cameras is non-trivial information for many computer visions applications. Different cameras usually produce differently-colored images for the same scene, regardless of how well adjusted the white balance is, due to the difference in the spectral sensitivity.

(a) Canon EOS Kiss. (b) Nikon D1.

Figure 1.2: Images captured with same camera parameters under same illumination condition: (a) Image captured by Kiss Digital X. (b) Image captured by Nikon D1.

Spectral sensitivity is the response of a sensor to monochromatic light as a functions of wavelength, also known as spectral response. This paper defines the spectral sensitivity on each *RGB* channel with the wavelength varying from 380 nanometers to 780 nanometers. The spectral sensitivity is normalized among three channels, therefore the maximum value is 1.0. Figure 1.2 shows the difference of two images which are captured by different cameras with same parameters (exposure time, F number, ISO) under same illumination environment. However, we can see that the appearance of this object looks so different because of the difference in spectral sensitivity characteristics of digital cameras.

Spectral sensitivity can be measured by dividing the image intensity by the corresponding spectra with two special equipments, spectrometer and monochrometer. Vora et al. [32] measured the spectral sensitivity of two digital cameras: Kodak DCS-200 and Kodak DCS-420 in this way. Image intensity is not linearly related to scene radiance recorded at the camera sensor, it must be linearized first in order to calculate the spectral sensitivity. In this paper, the camera response function is determined by stimulating the camera with varying intensities of a single light source obtained with ND filters (neutral density filters). The image intensity of camera Kodak DCS-200 was verified to be linear over most of the visible spectra range, a linearization curve of camera Kodak DCS-420 was also developed. The spectral sensitivity for these cameras are determined by stimulating them with very narrow-band illumination produced by a monochrometer, while simultaneously capturing the images and spectra by these cameras and the spectrometer, respectively. This measurement is conceptually very simple and can be very accurate. However, the equipment required to produce sufficiently intense narrow-band illumination at uniformly spaced wavelengths is expensive and not readily available.

1.2 Thesis Overview

Chapter 2 describes the proposed method for estimating diffuse reflectance parameters of an outdoor object with the presence of inter-reflection. After briefly reviewing the related work, the radiometric definitions and the calculation of radiance and irradiance value are introduced. Then, the inter-reflection model based on [3] is explained. The inter-reflection problem is solved by making an assumption that the object surface consists of hundreds of small facets. The inter-reflection effect on one facet is calculated as the sum of incoming light energy from all the other facets. The problem caused by occlusion between two facets is also solved. The occlusion between two facets affects the estimated reflectance so much that it makes the synthesized image appears very dark. The chapter solves the occlusion problem by detecting the vector between two facets intersects with another facet or not. If the intersection exists, the inter-reflection between these two facets is not calculated. The reflectance of each facet is calculated based on this inter-reflection model. Experimental evaluation on both simulation and real outdoor objects shows the improvement achieved by the proposed method.

Chapter 3 proposes a method for estimating the spectral sensitivity of digital cameras by using basis functions which are extracted from database by SVD (Singular Value

Decomposition). Related work is introduced first, then the benefits of using basis functions for sensitivity estimation are explained. In order to extract the basis functions, we measured the spectral sensitivity of digital cameras and collected from literature to create a database. The chapter verifies the accuracy of collected sensitivities by analyzing the error between the measured RGB values and predicted values which are calculated from spectra. The basis functions are extracted from the database by SVD method. This chapter compares the extracted basis functions with another three different mathematical basis functions, the polynomial basis functions, the Fourier basis functions and radial basis functions to obtain the optimum set of basis functions. The evaluation result shows that the extracted basis functions are reliable and adequate for estimating the spectral sensitivity of an arbitrary digital camera.

Chapter 4 concludes this dissertation by summarizing this thesis and contributions, and discussing possible future research directions.

Chapter 2

Reflectance Estimation with the Presence of Inter-reflection

Computer vision and graphics techniques need the accurate reflectance properties to create a realistic three-dimensional model of a real world object. This chapter proposes a practical method to estimate the surface reflectance parameters of outdoor diffuse object with the presence of inter-reflection. The inter-reflection problem is solved by making an assumption that the object surface consists of hundreds of small facets. The inter-reflection effect on one facet is calculated as the sum of incoming light energy from all the other facets. The problem caused by occlusion between two facets is also solved. The occlusion between two facets affects the estimated reflectance so much that it makes the synthesized image appear very dark. The chapter solves the occlusion problem by detecting the vector between two facets intersects with another facet or not. If the intersection exists, the inter-reflection between these two facets is not calculated. Experimental evaluations on both simulation and real outdoor object show the improvement achieved by the proposed method.

2.1 Introduction

To create a realistic model of a real world object by computer vision and graphics techniques has attracted interest from a wide range of research fields and industries in recent years. Shape and reflectance properties of the object are necessary to simulate the accurate appearance of an object. As a result of significant advancement of range

sensors and data processing algorithms, shape of an object becomes acquirable without much difficulties [1] [2]. However, obtaining the reflectance properties of the object remains a challenge, because the reflectance properties of a real object are usually very complicated.

One reason of this complexity is the inter-reflection between object surfaces. Light rays that we observe is the result of reflections repeated between surfaces infinitely. It is difficult to trace back those recursive reflections from the observation, and therefore, only few works that handle inter-reflections with regards to reflectance estimation have been proposed.

This chapter proposes a practical method to estimate the reflectance parameters of an outdoor diffuse object with the presence of inter-reflection which based on the technique addressed by Nayar et al. [3]. Assuming that the object surface consists of hundreds of small facets, the inter-reflection effect on one facet is calculated as the sum of incoming light energy from all the other facets. Experimental evaluations on both simulation and real outdoor object show the accuracy of proposed method.

2.1.1 Related Work

In the late 1990s, textures of an object were modeled by linearly combining multiple reference textures [5] [6] [7] [8] [9]. In order to create more realistic and physically correct model of an object, a lot of methods have been proposed in the last two decades, such as physics-based reflectance parameter estimations [10] [11] [12], and image-based renderings [13] [14].

The early work related to inter-reflection has been done by Nayar et al. [3]. They estimated the shape and surface reflectance of a concave object, which has a lot of inter-reflections inside. In this method, the object is assumed to have a uniform surface reflectance. Another inverse-global-illumination method is proposed by Yu and Debevec [4]. This method is applied for an indoor room, and it requires images from different view points to cover the whole room. The light positions have to be known in the method.

Sato and Ikeuchi [15] proposed a method to estimate reflectance properties by taking a number of images under varying illumination conditions. The method estimates accurate reflectance of both diffuse and specular components. Nayar et al. [16] developed a technique to separate the direct and global components of a scene using high frequency illumination. The direct component means the brightness of a scene whose

radiance value is directly due to the light source, while the global component represents radiance value due to the other points in the scene. By projecting two complement patterns to illuminate the objects, the direct and global components can be separated. Those methods are only applicable for indoor objects.

Weiss [17] proposed a method to separate the illumination and reflectance of an outdoor scene by using the derivate filter. The method requires a sequence of images of a whole day, and does not take the inter-reflection into account.

2.1.2 Radiometric Definitions

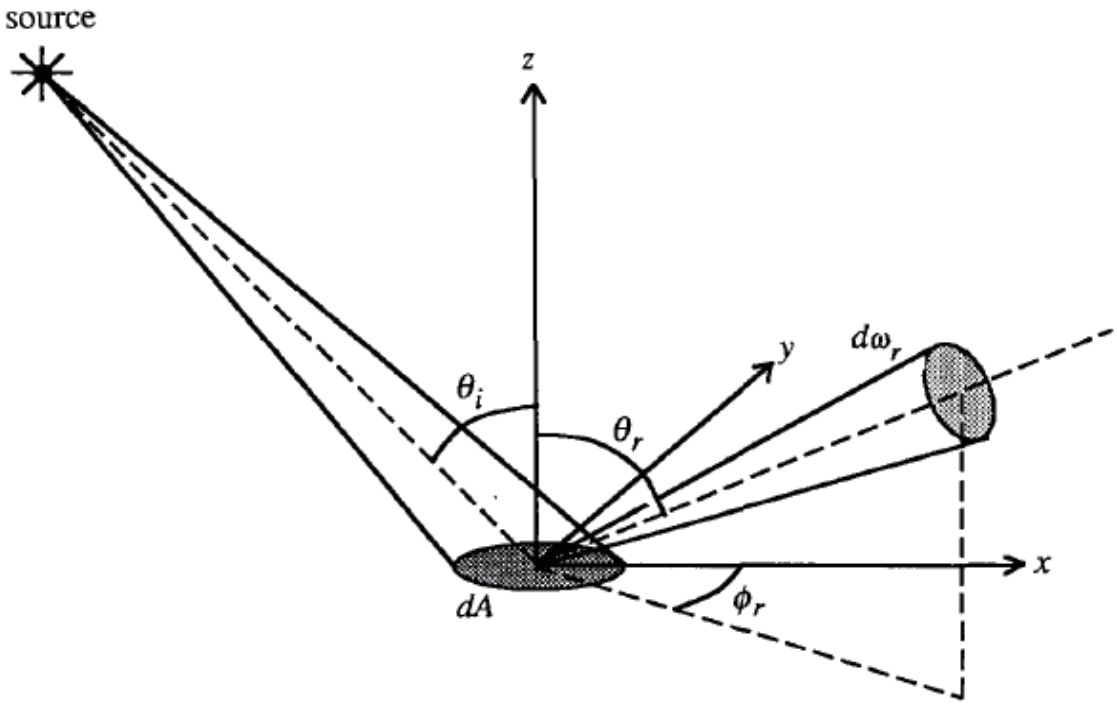

Figure 2.1: Geometry used to define radiometric terms [3].

Definitions of radiometric terms which are used in the analysis of inter-reflection are described as follows (detailed derivations of these terms are given by Nicodemus et at. [41]). Figure 2.1 shows a surface element illuminated by a source light. The irradiance E of the surface is defined as the incident flux density (W/m^2):

$$E = \frac{d\Phi_i}{dA} \tag{2.1}$$

where $d\Phi_i$ is the flux incident on the area dA of the surface facet. The radiance L of the surface is defined as the flux emitted per unit foreshortened area per unit solid angle ($W/m^2/sr$). The surface radiance in the direction (θ_r, ϕ_r) is determined as

$$L = \frac{d^2\Phi_r}{dAcos\theta_r d\omega_r} \tag{2.2}$$

where $d^2\Phi_r$ is the flux radiated within the solid angle $d\omega_r$. The Bidirectional Reflectance Distribution Function (BRDF) of a surface is a measure of how bright the surface appears when viewed from one direction while it is illuminated from another direction. The BRDF is described as:

$$f = \frac{L}{E} \tag{2.3}$$

2.2 Radiance and Irradiance Value of Object Surface

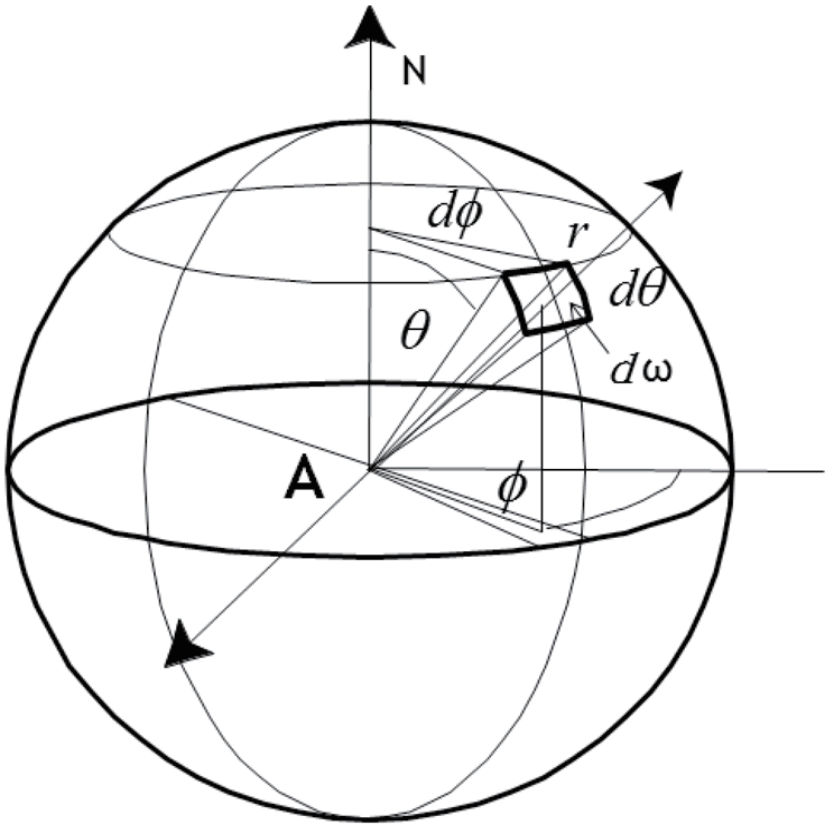

Figure 2.2: Calculation of radiance and irradiance value

In general, when assuming the object surface is Lambertian and there is no inter-reflection, the reflectance of an object can be derived from the bidirectional reflectance distribution function $f = \frac{L}{E}$, where L and E are the radiance and irradiance values of object surface, respectively.

Consider a facet located at the center of the sphere (as shown in Figure 2.2), then the solid angle $d\omega$ can be derived from the elevation θ and azimuth ϕ:

$$d\omega = \sin\theta d\theta d\phi \tag{2.4}$$

The energy received by the facet A from a particular direction, surrounded by an infinitesimal solid angle $d\omega$, is described as:

$$L(\lambda, \theta, \phi)\cos\theta \sin\theta d\theta d\phi \tag{2.5}$$

where $L(\lambda, \theta, \phi)$ is the incident radiance distribution of illumination.

The irradiance value of the facet A can be expressed as the integral of incident energy over the hemisphere whose north pole is at the surface normal direction:

$$E^A = \int_{-\pi}^{\pi}\int_{0}^{\frac{\pi}{2}} L(\lambda, \theta, \phi)\cos\theta \sin\theta d\theta d\phi \tag{2.6}$$

In this chapter, we assume that the object surface is Lambertian surface, and therefore the reflected light is isotropic. Then, the radiance value of the facet A is expressed as the multiplication of irradiance value E and reflectance S^A:

$$I^A = \int_{-\pi}^{\pi}\int_{0}^{\frac{\pi}{2}} S^A L(\lambda, \theta, \phi)\cos\theta \sin\theta d\theta d\phi \tag{2.7}$$

2.3 Inter-reflection Model

The inter-reflection effect especially for the concave object is not negligible. In order to acquire the accurate reflectance properties for 3D object, we addressed an inter-reflection model to calculate the inter-reflection effect. An assumption is made that the object surface consists of hundreds of small facets as shown in Figure 2.3. The inter-reflection effect on each facet is calculated as the sum of incoming light energy from all the other facets.

When the surface of a concave object is illuminated, its facets receive light from both light source and other facets, as shown in Figure 2.4. In Figure 2.4, the small facet x receives light from both light source and another facet $x\prime$ on the surface. Therefore,

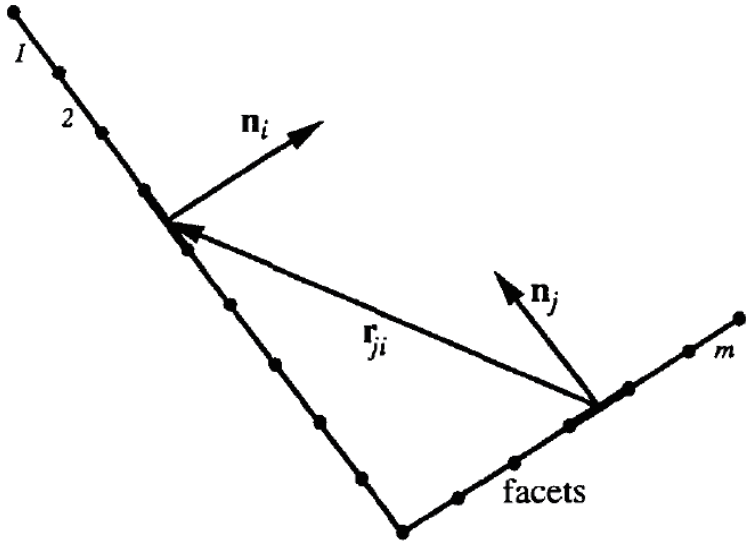

Figure 2.3: Modeling the surface as a collection of facets, each with its own radiance and reflectance values [3].

the radiance value at each surface facet has two components, one directly resulting from the light source and the second due to illumination by other facets. The latter component is also called as inter-reflection effect.

Radiance due to other facets The inter-reflection effect between two facets i and j is strongly affected by whether these two facets can see each other or not. Two facets i and j which are visible to each other is shown in Figure 2.5. The visibility V between two facets i and j is determined by the following function:

$$V_{ij} = \frac{n \cdot (-r) + |n \cdot (-r)|}{2|n \cdot (-r)|} \cdot \frac{n\prime \cdot r + |n\prime \cdot r|}{2|n\prime \cdot r|} \cdot Occ \tag{2.8}$$

where n and $n\prime$ are unit surface normals of the ith and jth facets, r is the vector from jth to ith facet, and Occ is the coefficient for occlusion between these two facets. If the ith and jth facets are occluded by another facet, these two facets can not see each other.

The occlusion coefficient is important to calculate the visibility function. A typical situation when occlusion happens is shown in Figure 2.6. In Figure 2.6, the ith facet lies on the horizontal top plane, while the jth facet lies on the vertical plane. Since there is another horizontal plane between them, they cannot see each other and there is no inter-reflection effect between ith and jth facets. The occlusion coefficient is calculated as follows: for the vector between the ith and jth facets, we detect whether this vector intersects with another facet or not. If the vector intersects with at least one of the other

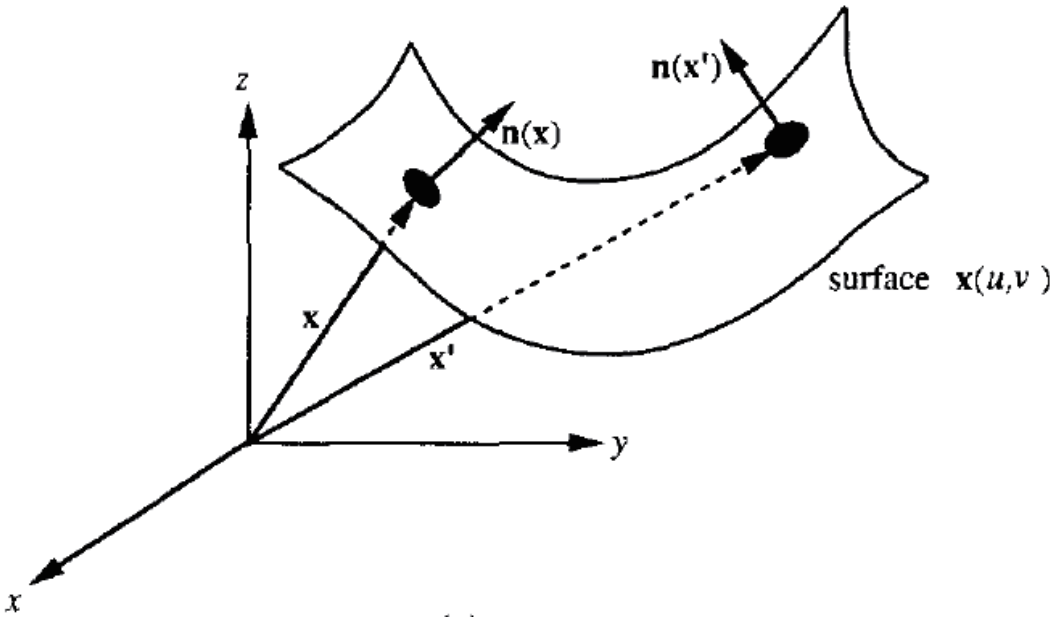

Figure 2.4: A concave surface in three-dimensional space [3].

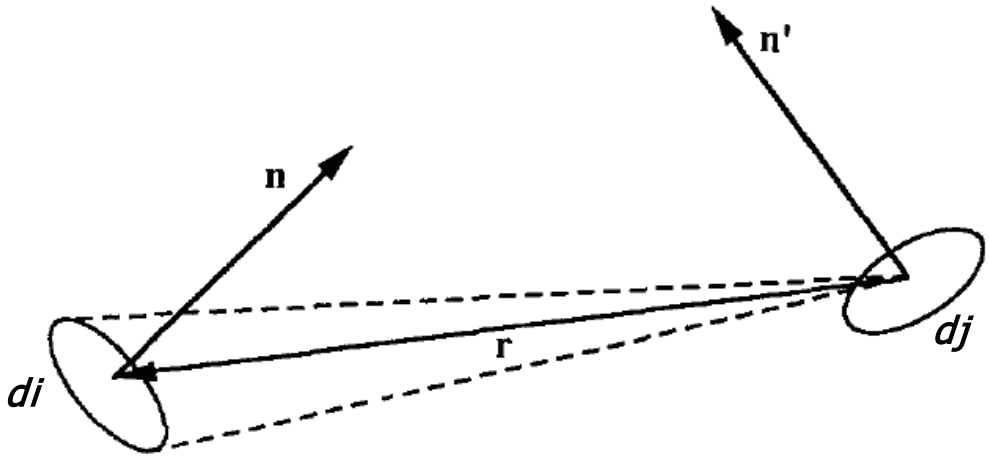

Figure 2.5: Two surface elements that are visible to one another.

facets, the occlusion coefficient is equal to zero. If not, there is no occlusion between the ith and jth facets and the occlusion coefficient is set to one.

The visibility function V_{ij} in Equation (2.8) can only have two values, 1 or 0. If it is equal to 1, the ith and jth facets see each other and the inter-reflection between these two facets will be calculated. If not, no inter-reflection exists between the facets.

Let E_{ij} be the irradiance value of ith facet due to the radiance value of the jth facet L_j. E_{ij} can be derived from the definitions of radiance and irradiance and geometry shown in Figure (2.5):

$$E_{ij} = [\frac{[n \cdot (-r)][n\prime \cdot r]V_{ij}}{[r \cdot r]^2}]L_j S_i \tag{2.9}$$

where S_i is the area of the ith facet, V_{ij} is the visibility function between the ith and jth facets, and L_j is the radiance value of the jth facet.

The radiance value L_{ij} of the ith facet can be determined from its irradiance value E_{ij} as:

$$L_{ij} = \frac{\rho_i}{\pi} E_{ij} \tag{2.10}$$

where ρ_i is the reflectance of the ith facet. The reflectance is assumed to be invariable among a facet, since a facet size is sufficiently small. The factor $\frac{\rho_i}{\pi}$ is the bi-directional reflectance distribution function for a Lambertian surface. From Equations (2.9) and (2.10), we obtain

$$L_{ij} = \frac{\rho_i}{\pi} K_{ij} L_j \tag{2.11}$$

where

$$K_{ij} = [\frac{[n \cdot (-r)][n\prime \cdot r]V_{i_j}}{[r \cdot r]^2}]S_i \tag{2.12}$$

K_{ij} is a coefficient determined by the positions and orientations of the ith and jth facet.

From Equation (2.11), we obtain the radiance value L_{ij} of ith facet due to the radiance value of jth facet, and as described before, this radiance value is the second component of the total radiance value for a small facet lies on the surface of a concave object.

Radiance due to a light source The radiance value of the ith facet directly due to a single point light source (excluding interreflection effect) can be expressed by using the irradiance value:

$$L_{si} = \frac{\rho_i}{\pi} E_{si} \tag{2.13}$$

where E_{si} is the irradiance value of the ith facet directly due to a light source. The irradiance value can be calculated from Equation (2.6).

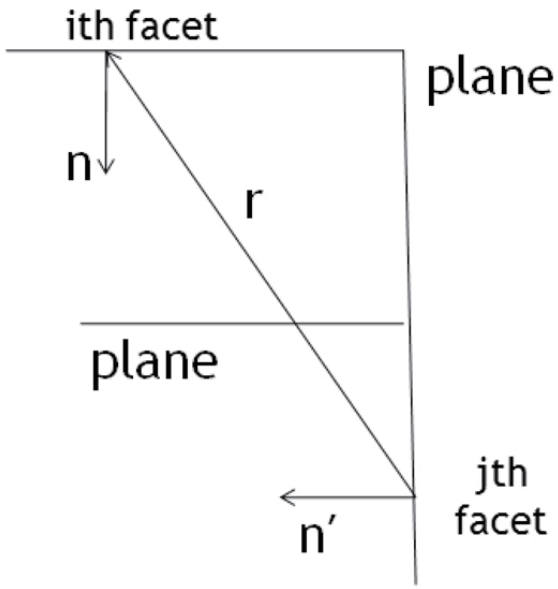

Figure 2.6: Occlusion between two facets: the ith and jth facets are occluded by the middle horizontal plane

Total radiance The total radiance value of the ith facet L_i can be expressed as a sum of the radiance due to a light source L_{si} and all the other facets on the surface:

$$L_i = L_{si} + \frac{\rho_i}{\pi} \sum_{j=1}^{m} L_j K_{ij} \tag{2.14}$$

where m is the number of facets on the object surface. When j equals to i, the K_{ij} coefficient between the ith and jth facets becomes zero, according to Equation (2.12).

The inter-reflection equation for a concave surface can be written as follows using a vector notation. Let us define the facet radiance vector as $L = [L_1, L_2, ..., L_m]^T$, the source contribution vector as $L_s = [L_{s1}, L_{s2}, ..., L_{sm}]^T$, and the reflectance matrix P and the K_{ij} coefficient matrix K as:

$$P = \frac{1}{\pi} \begin{bmatrix} \rho_1 & 0 & \cdots & 0 \\ 0 & \rho_2 & \cdots & 0 \\ \cdots & \cdots & \cdots & \cdots \\ \cdots & \cdots & \cdots & \cdots \\ 0 & 0 & \cdots & \rho_m \end{bmatrix} \tag{2.15}$$

$$K = \begin{bmatrix} 0 & k_{12} & \cdots & \cdots & \cdots \\ k_{21} & 0 & \cdots & \cdots & \cdots \\ \cdots & \cdots & 0 & \cdots & \cdots \\ \cdots & \cdots & \cdots & 0 & \cdots \\ \cdots & \cdots & \cdots & \cdots & 0 \end{bmatrix} \tag{2.16}$$

Now, the Equation (2.14) can be written as:

$$L = L_s + PKL \tag{2.17}$$

The reflectance matrix P can be derived from Equation (2.17) as:

$$P = (L - L_s)L^{-1}K^{-1} \tag{2.18}$$

The parameters of matrix P are the reflectance of each facet, and can be obtained as:

$$\rho_i = \pi L_i(E_{si} + L_1K_{i1} + L_2K_{i2} + ... + L_mK_{im})^{-1} \tag{2.19}$$

where ρ_i is the reflectance of the ith facet, L_i is the radiance value of the ith facet, E_{si} is the irradiance value due to the light source, and K_{ij} is a coefficient between the ith and jth facets. The irradiance and radiance values can be calculated from Equations (2.6) and (2.7), respectively. The K coefficient is determined only by the geometry of two facets on the object surface, and can be derived from the object shape. From Equation (2.19), we can acquire the reflectance of each facet on the object surface with the presence of inter-reflection.

2.4 Experiment

In this section, we will show our experimental results for both simulation and real outdoor objects with the presence of inter-reflectons. As described before, the inter-reflection effect on a facet can be calculated as the sum of incoming light energy from all the other facets by assuming that the object surface consists of hundreds of small facets. The experimental evaluations show the improvement achieved by proposed method.

2.4.1 Simulation Object

First we applied our method to estimate the reflectance of a simulation object. We use the Radiance software [42] to define two planes perpendicular to each other. One and the other plane have the reflectance of (0.1, 0.2, 0.7) and (0.7, 0.1, 0.1) for the three RGB channels, respectively. After rendering using Radiance software, the acquired image is the radiance image of the defined object. This image can be also called as observation, the pixel value of observation is the radiance value of corresponding facets.

The irradiance value of a small facet due to light source (E_{si} in Equation (2.19)) is proportional to cosine of the angle between the source direction and the surface normal direction of the small facet, that is $E_{si} = kn \cdot s$. The constant of proportionality k is determined by the radiant intensity of the source and its distance from the surface. Then, in Equation (2.19), for each facet, we can read the radiance value from the observation, calculate the irradiance value as the multiplication of constant k and dot production, also the K_{ij} coefficient can be calculated from Equation (2.12).

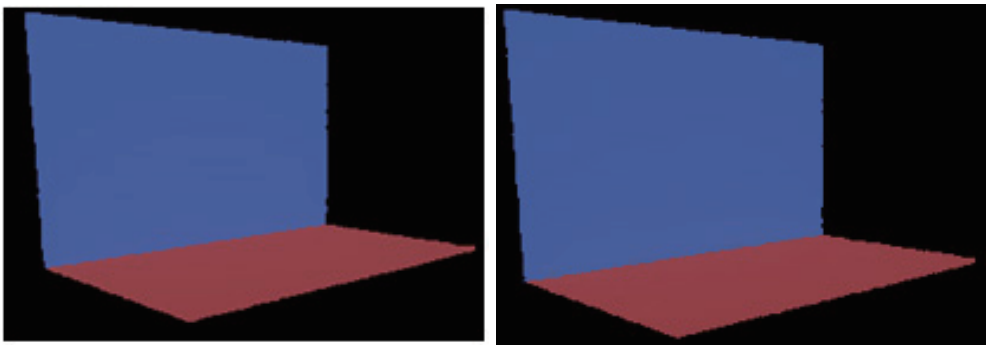

(a) Observation. (b) Synthesized image.

Figure 2.7: (a) Radiance image of simulation object (b) Synthesized image rendering with the estimated reflectance

Figure 2.7(a) shows the simulation object. We use the estimated reflectance and the same light condition to re-render the simulation object, and get the synthesized image of this object. This synthesized image is shown in Figure 2.7(b). Figure 2.8 shows the difference between the observation and the synthesized image. The difference is less than 4 percent for two planes. This means the pixel value of synthesized image is similar to observation.

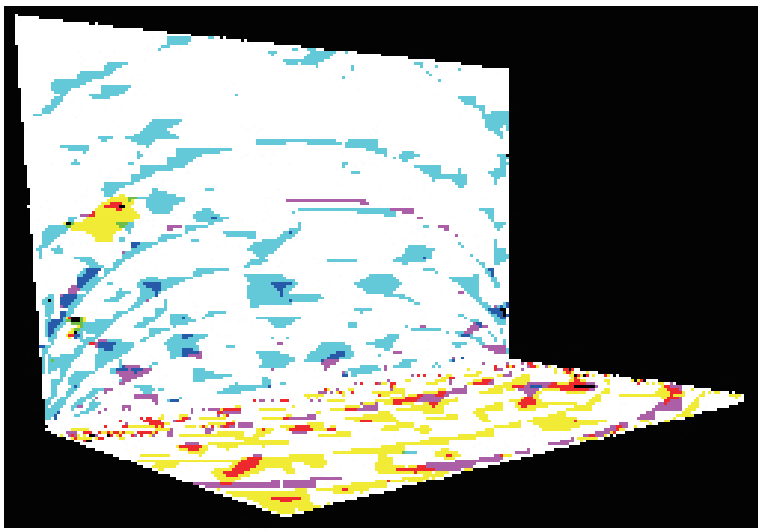

Figure 2.8: Difference image (10 times brighter) between observation and synthesized image

Figure 2.9: A spherical motion camera Ladybug2 [44]

2.4.2 Real Outdoor Object

For the experiment of real outdoor diffuse object, we choose the clock tower in Tokyo University campus. Unlike the simulation object, it is much harder to estimate the accurate reflectance of a real outdoor object, because the light source for an outdoor object can not be controlled. For light source of an outdoor object, we used image based lighting to render the object.

Observation capture and shape acquisition The proposed method for estimating the reflectance parameters of outdoor diffuse object only needs one measurement with a spherical camera. The camera we used is Ladybug2 [44] as shown in Figure 2.9. Ladybug2 has 6 lenses, one of them and the others point to vertical and horizontal directions. This camera could capture nearly 75 percent of a 360-degree field of view; thus, it captures the radiance of an object and illumination environment at one shot. Using the same camera sensitivity for capturing the object and illumination, the algorithm becomes simple and no calibration of the camera gain factor is needed. It is always sure that the image intensity of the object reflects the instantaneous response to the surrounding illumination that is captured in the same image. The camera pose calibration is required only once; the object and illumination are geometrically consistent in the acquired image.

To capture the wide level of intensity, we took images with ND filters and multiple shutter speeds. We used two ND filters, Fujifilm ND-4.0 and ND-3.0 that reduce incoming light to 1/10000 and 1/1000, respectively. Each filter was placed in front of the lenses. We also tuned the shutter speeds carefully to cover the entire dynamic range in conjuction with these filtes, and took images, as Figure 2.10 shows.

The ND filters attached in front of the lens produce vignette-like effect. Image brightness gradually reduces from the center towards the periphery of the image, as Figure 2.11 (a) shows. This is due to the reflection at the interface of the ND filter. Light that is reflected by the filter increases when its incident angle is off the optical axis.

To rectify the reduction of image brightness, we took images of a white board by Ladybug2 with and without the ND filter. In this experiment, images from each camera lens were output. Then, we modeled the effect by an empirical mathematical model, and calculated the parameter by the least square fitting. Figure 2.11 (b) shows the estimated vignetting effect. By dividing the images taken with ND filter by Figure 2.11 (b), rectified images can be acquired, as shown in Figure 2.11 (c).

The rectified observation is shown in Figure 2.11 (c). The image's vertical and

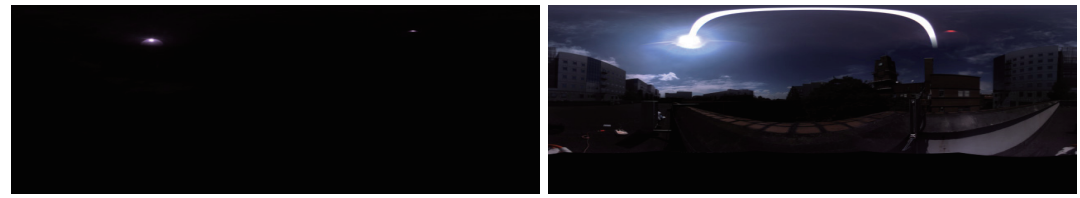

Shutter speed: 1/39, with ND-4.0 filter Shutter speed: 1/10000

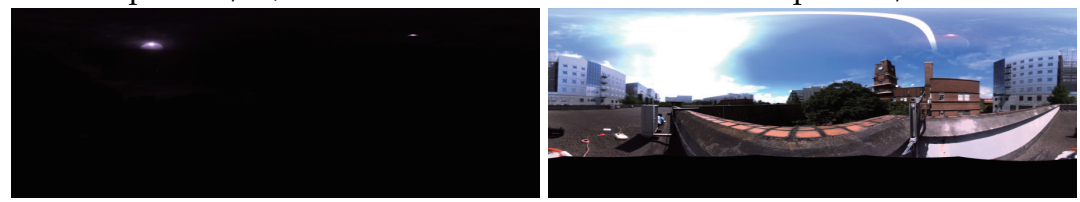

Shutter speed: 1/19, with ND-4.0 filter Shutter speed: 1/2500

Shutter speed: 1/9, with ND-4.0 filter Shutter speed: 1/1250

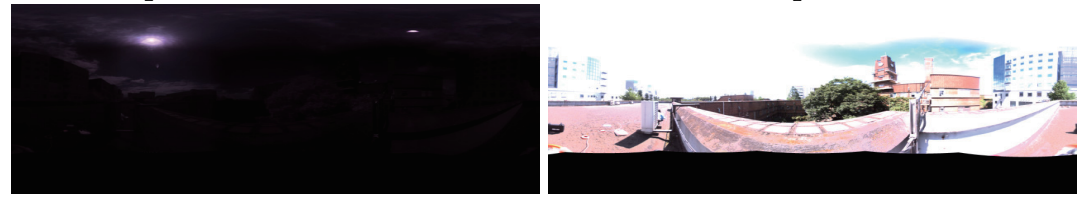

Shutter speed: 1/5, with ND-4.0 filter Shutter speed: 1/625

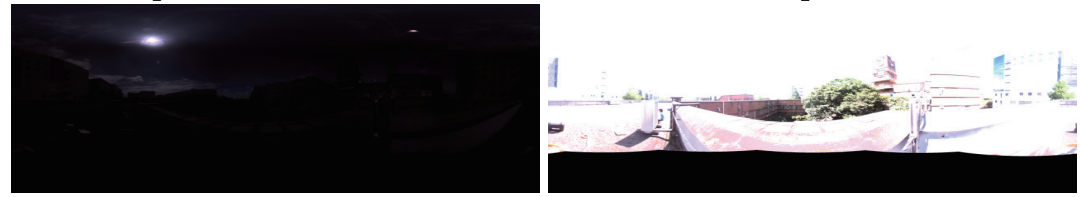

Shutter speed: 1/39, with ND-3.0 filter Shutter speed: 1/312

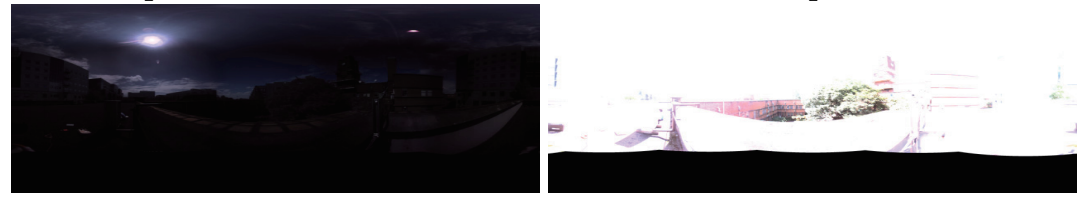

Shutter speed: 1/19, with ND-3.0 filter Shutter speed: 1/156

Figure 2.10: A set of images taken on a sunny day. The unit of shutter speeds is micro second. Normally, about twenty and ten images were taken on sunny and cloudy days, respectively.

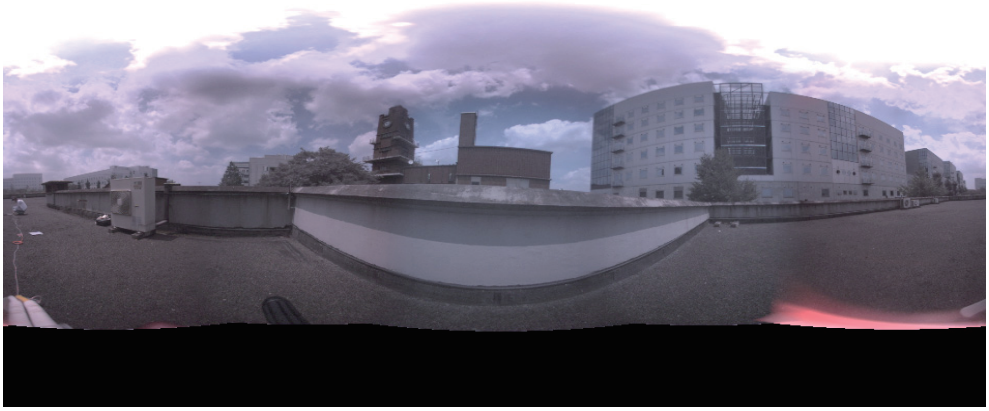

(a)

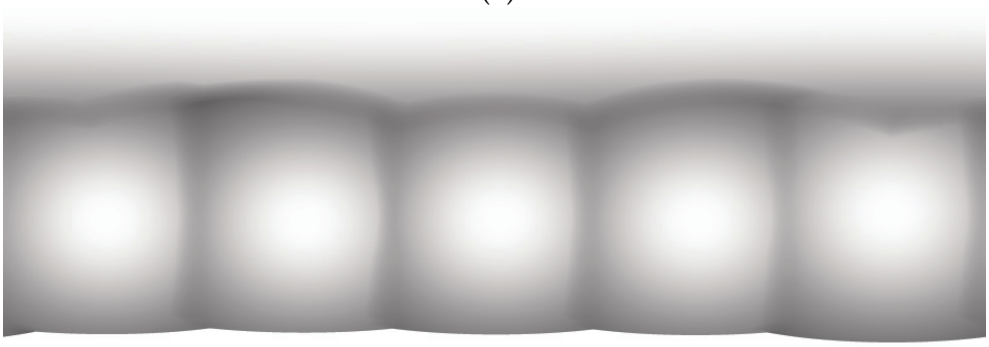

(b)

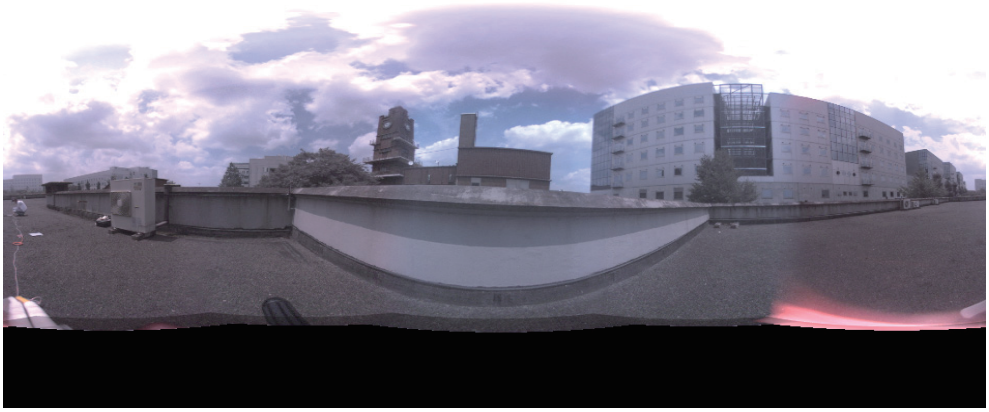

(c)

Figure 2.11: (a): an image with vignette-like effect. See the upper right of the image. The reduction of image is highly visible. (b): the estimated vignette-like effect. (c): an image rectified. Image brightness is recovered.

Figure 2.12: The range sensor Cyrax 2500 [43] used to acquire the shape information.

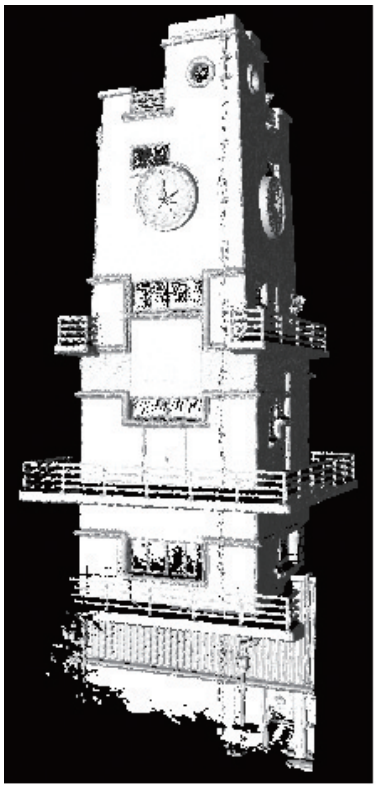

Figure 2.13: Acquired shape information of clock tower by Cyrax 2500.

horizontal axes correspond to the polar and zenith angles. The camera captures nearly 75 percent of a 360-degree field of view, so it captures the radiance distributions of the sky and the target object at a time.

The object shape information is acquired by the range sensor Cyrax 2500 [43]. This range sensor has a maximum $40^\circ \times 40^\circ$ field-of-view. With a single-point range accuracy of +/- 4mm, angular accuracies of +/- 60 micro-raians, and a beam spot size of only 6mm from 0-50m range, the Cyrax sensor delivers survey-grade accuracy while providing a versatile platform for data capture. Figure 2.12 shows the range sensor Cyrax 2500. The acquired shape of clock tower is shown in Figure 2.13. From the shape, we can get the surface normal and 3D coordinates of each facet on the object surface to calculate the inter-reflection effect.

We calibrated the object and the camera coordinates using Tsai's method [54]. We found corresponding points between the shape of the object and the images taken, then we calculated the view point and the projection matrix using those coordinate pairs.

Figure 2.14: Radiance image of clocktower which is cut from the observation.

Radiance calculation In the experiment of clock tower, the radiance value of each facet is read from the radiance image. The radiance image which is cut from the

rectified observation (as shown in Figure 2.11 (c)) is shown in Figure 2.14.

Irradiance calculation The irradiance value directly due to the light source can be calculated from Equation (2.6). In this experiment, we used Radiance software to do the irradiance calculation. Specifically, first we set the reflectance of each facet to be 1.0 for all the RGB channels, then render the clock tower by image based lighting method. The image rendered is the irradiance image, as shown in Figure 2.15.

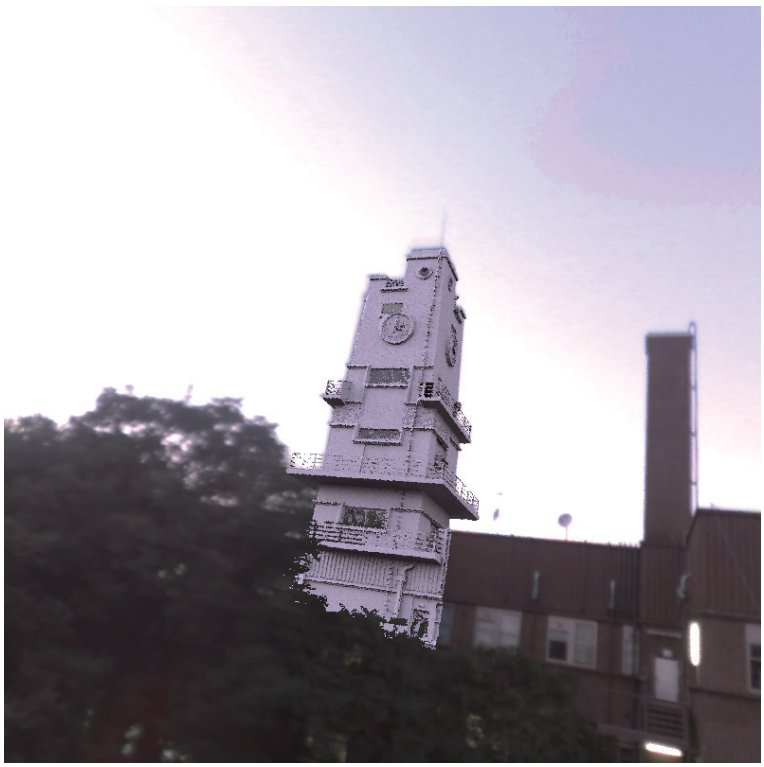

Figure 2.15: Irradiance image of clocktower

Reflectance estimation Known the surface normal and three dimensional coordinates of each facet from acquired shape, the K_{ij} coefficient can be calculated from Equation (2.12). By using the radiance value read from the radiance image of clocktower which is cut from the observation and irradiance value calculated from Equation (2.6), we can calculate the reflectance of each facet according to Equation (2.19).

As shown in Figure 2.6, even though the visibility function without occlusion coefficient between these two facets is equal to 1, these two facets actually can not see each other because of the occlusion. Figure 2.16 shows this kind of situation.

(a) K coefficient. (b) K coefficient.

Figure 2.16: (a)K coefficient calculation with occlusion (b) K coefficient calculation without occlusion

When estimating the reflectance of the small facet lies in the blue circle, the K_{ij} coefficient is calculated between this facet and all the other red facets shown in Figure 2.16(a). Apparently, there are too many red facets that this facet actually can not see. But the K_{ij} coefficient was included in the sum as inter-reflection effect because of the occlusion between them. Without occlusion coefficient, the calculated inter-reflection effect would be too large, the estimated reflectance would be too small. We solve this occlusion problem by applying the occlusion coefficient to visibility function calculation. Specifically, we detect whether the vector between the ith and jth facets intersects with all the other facets or not. If the vector intersects with at least one of the other facets, then the occlusion coefficient is equal to 0, so is the K_{ij} coefficient. If not, the visibility function is equal to 1, and the K_{ij} coefficient can be calculated from Equation (2.12).

Figure 2.16(b) shows the situation when dealing with the occlusion problem by the method described before. The red facets have the same meaning as Figure 2.16(a). For the same facet, the number of red facets in Figure 2.16(b) is only around one third of Figure 2.16(a). Two thirds of red facets in Figure 2.16(a) are occluded, and should not be seen by the facet lies in the blue circle. With the occlusion coefficient, the estimated reflectance becomes much more accurate.

In order to evaluate the estimated reflectance, we used the image based lighting method to render the clock tower, the result is shown in Figure 2.17.

Figure 2.17(a) is the observation of clock tower, (b) is the result re-rendered by the previous method which does not take the inter-reflection effect into account, (c) is the result re-rendered by our proposed method. From Equations (2.6) and (2.7), if we divide the radiance value by the irradiance value of each facet, we can estimate the reflectance, however this does not handle the inter-reflection effect. Okura et al. [45] used this method to estimate the reflectance of an outdoor diffuse object. Figure 2.17(b) was rendered by this way, there is no inter-reflection effect calculated for each facet on the object surface. Figure 2.17(c) shows the synthesized image re-rendered with estimated reflectance, which are obtained by our proposed method.

Figures 2.18(a) and (b) show the difference between observation of clock tower (Figure 2.17(a)) and synthesized image without inter-reflection effect (Figure 2.17(b)) and with inter-reflection effect (Figure 2.17(c)), respectively. From the comparison between Figures 2.18(a) and (b), for most concave parts of clock tower, if handling the inter-reflection effect, the re-rendered image looks much more realistic. The difference between the re-rendered image with inter-reflection effect and radiance image of clock

(a) Truth value.(b) No inter-reflection. (c) Inter-reflection.

Figure 2.17: (a) Observation of clock tower (b) Synthesized image without inter-reflection (c) Synthesized image with estimated reflectance

tower, especially for the concave parts, is less than three percent. But for re-rendered image without inter-reflection effect, the difference is bigger than sixty percent.

In order to make it clear, we zoom in the red rectangle part in Figure 2.18 (a) and (b). The amplified result is shown in Figure 2.19 (a) and (b). In these Figures, the *RGB* values of the pixel (brightness) represents the error. If the error is larger, the pixel will be brighter. Obviously, the result estimated by our proposed method (as shown in Figure 2.19 (b)) has much smaller errors. We took four pixels (the red, green, blue and yellow pixel as shown in Figure 2.19 (a) and (b)) as examples, the difference for these four pixels between the observation and re-rendered image without inter-reflection effect and with inter-reflection effect are shown in Table 2.1. Except the yellow pixel, the other three pixels of our proposed method have much smaller errors. The error for yellow pixel is larger compared to error of other pixels, because actually it is occluded by the tree which lies in front of the clock tower (as shown in Figure 2.14). The geometrical and optical information of this yellow pixel does not match. For the blue pixel which has strong inter-reflection effect, the error of Okura's method which does not take the inter-reflection into account is almost 15 times bigger than the error of our proposed method. This proves the efficiency of proposed method.

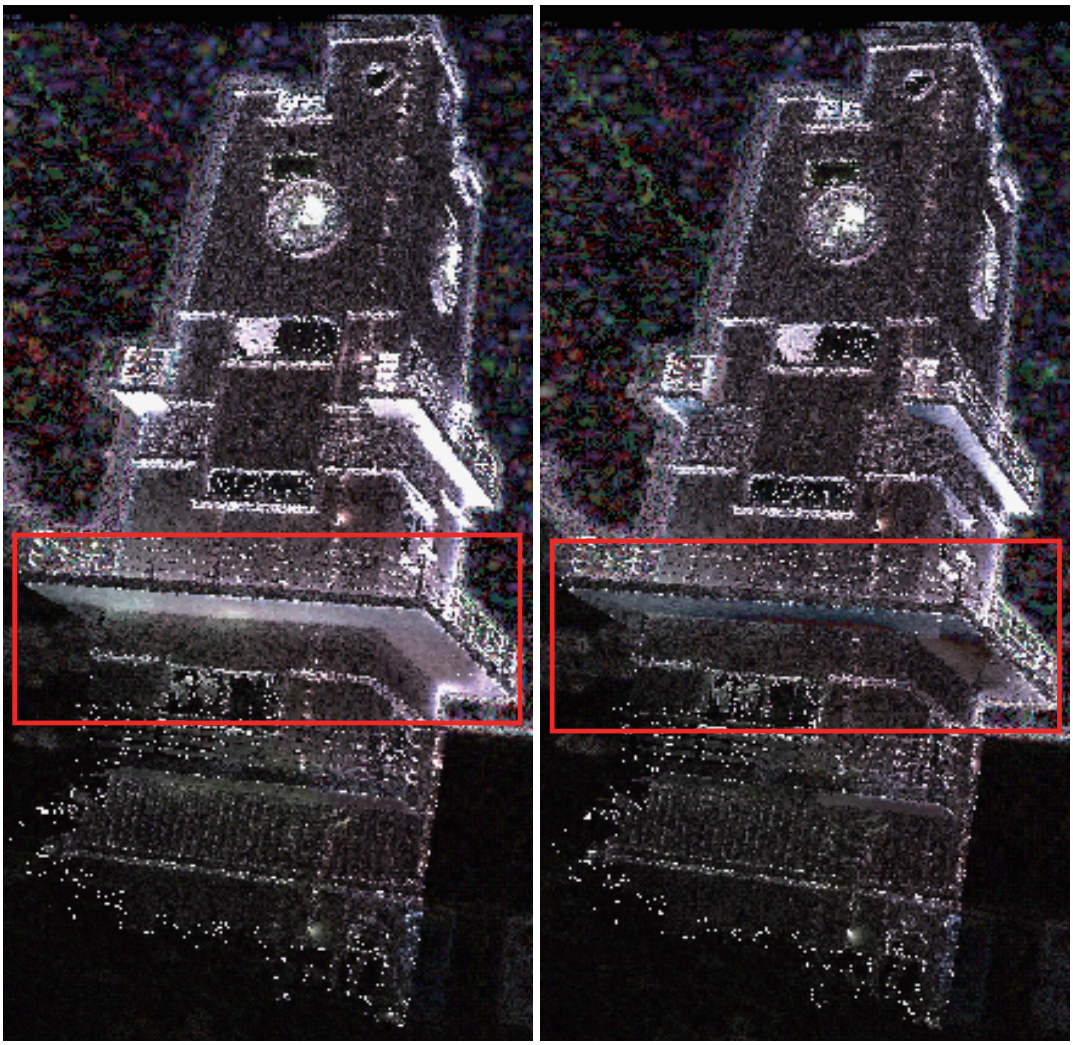

(a) No inter-reflection. (b) Inter-reflection.

Figure 2.18: (a) Difference between observation and re-rendered image without inter-reflection (b) Difference between observation and re-rendered image with inter-reflection

(a) Zoom in of result without inter-reflection.

(b) Zoom in of result with inter-reflection.

Figure 2.19: (a) Difference of zoomed in part between observation and re-rendered image without inter-reflection (b) Difference of zoomed in part between observation and re-rendered image with inter-reflection

Table 2.1: Difference of zoomed in part of Okura's method (without inter-reflection effect) and our proposed method (with inter-reflection effect)

Pixels	Okura's method	Our proposed method
Red pixel	0.042	0.009
Green pixel	0.066	0.007
Blue pixel	0.102	0.007
Yellow pixel	0.048	0.014

In the re-rendered image with estimated reflectance by our proposed method (as shown in Figure 2.17(c)), there are some parts which still have large errors and many highlight points. We consider that these errors might be caused by lack of whole geometry and calibration error between three-dimensional object and two-dimensional image.

2.5 Summary

This chapter explains our proposed method to estimate the reflectance properties of outdoor diffuse object with the presence of inter-reflection. This problem is solved by assuming the object surface consists of hundreds of small facets. The inter-reflection effect on each facet is calculated as the incoming energy from all the other facets. This technique takes shape and radiance image as input to estimate the reflectance of object surface. Then, the estimated reflectance can be used for synthesizing image. This chapter also solves the problem caused by occlusion between two facets by detecting the vector between two facets intersect with another facet for not, the occlusion affect the estimated reflectance so much that it makes the synthesized image appear very dark. In the experiment, the shape information is acquired by the range sensor Cyrax 2500, and a spherical motion camera Ladybug2 is used to capture the radiance image. This spherical camera can capture the radiance of the object and illumination environment at one shot, this makes the algorithm of reflectance estimation become simple and no calibration of the camera gain factor is needed. The experimental evaluation shows the accuracy of proposed method. Compared to the re-rendered image without inter-reflection, result of our proposed method is much more similar to the real one.

Chapter 3

Camera Sensitivity Recovery

Spectral sensitivity of digital cameras plays an important role for many computer vision applications. However, previous work does not provide reliable estimation for spectral sensitivity. This chapter investigates the characteristics by extracting the basis functions of them by using SVD (Singular Value Decomposition); we measured the spectral sensitivity of different digital cameras and also collected data from the literature. The extracted basis functions are compared with different mathematical basis functions, the polynomial basis functions, the Fourier basis functions and the radial basis functions, to obtain the optimum set. The extracted basis functions can be used to estimate the unknown spectral sensitivity of an arbitrary camera.

3.1 Introduction

Spectral sensitivity of digital cameras is non-trivial information for many computer visions applications. Different cameras usually produce differently-colored images for the same scene, regardless of how well adjusted the white balance is, due to the difference in the spectral sensitivity. When the spectral sensitivities of those cameras are known, color of one camera can be converted into that of the other. This would help a number of applications based on colors such as object recognition, object detection, image retrieval, etc. Several other methods of physics-based vision require spectral sensitivity, such as demosaicing [18], color correction [19] and illuminant estimation algorithms [20] [21]. Spectral sensitivity is also an essential characteristic for color constancy method [48] [49] [50] [51] [52]. Most color constancy algorithms require an

estimation of camera responses to the real world with its many different surfaces and illumination conditions. Although it is conceivable to obtain camera responses for a large number of surfaces under a given illuminant, it is impractical to obtain this data for each camera. Furthermore, some algorithms require this data for each possible illumination, including combinations of several sources. It is thus far more effective to first obtain illuminant spectra and spectral sensitivity of cameras, then by using a camera model to predict camera responses.

This paper investigates basis functions for spectral sensitivity of digital cameras. In order to extract basis functions, the SVD (Singular Value Decomposition) is performed to the database, which is created from the measured sensitivities and collected data from the literature. The extracted set of basis functions are compared to mathematical basis functions, the polynomial basis functions, the Fourier basis functions and the radial basis functions, by applying them to recover the unknown spectral sensitivity from the set of image intensities and spectra. The evaluation result shows that the extracted basis functions are reliable and adequate to estimate the spectral sensitivity of an arbitrary digital camera.

3.1.1 Related Work

Spectral sensitivity of digital cameras could be derived from the quotient of image intensity and corresponding spectra. Because of the high dimensionality of spectral sensitivity, this method becomes unstable. Much effort has been made to estimate the spectral sensitivity robustly. These methods are categorized into two groups: the method which try to introduce various constraints for spectral sensitivity and the method which try to model the spectral sensitivity by parameters to reduce the dimension.

For the first category, Sharma and Trussell [33] [34] improved the estimated spectral sensitivity by introducing various constraints. The maximum allowable error as well as RMS error (between measured and calculated spectral sensivity from spectra) is used as a constraint. In addition, they also constrain a discrete approximation of the second derivate to promote a smooth solution. Finally, they constrain the response functions to be positive. They then observed that the constraint sets were all convex, and so they compute a resulting constraint set using the method of projection onto convex sets. Hubel et al. [35] also recognize that some form of smoothness is necessary for a good solution, and they investigated the Wiener estimation method, as described by Pratt

and Mancill [36], as a method for finding a smooth fit. They find that generally the method produced good results. However, this method produced negative lobes in the response functions and the authors briefly mentioned using the projection-onto-convex-sets method to remedy this problem. Barnard et al. [37] introduce positivity and unimodality constraints combined with several other constraints such as regularization smoothing and Fourier smoothing constraints to improve the accuracy of estimated spectral sensitivity. However, the spectral sensitivity calculation of these methods are complicated according to the introduced various constraints.

For the second category, Thomson et al. [38] proposed a method to estimate the spectral sensitivity of cameras by using a parametric model. The response characteristics of the color channels are fitted with basis functions of the Gram-Charlier expansion [39]; this probability law uses Hermite polynomials to describe departures from pure gaussian shape. The first two Hermite polynomials are used: each response distribution is treated as possibly skewed, possibly kurtosed Gaussian functions. This parametric model has five parameters: the peak wavelength, amplitude, and width of the Gaussian, together with the skewness and kurtosis terms. The spectral sensitivity estimation is identified as a nonlinear modelling task in which the parameters of the model are varied so as to minimize the error over the visible range of wavelength. Nonlinear fitting is performed using the Levenberg-Marquardt (L-M) technique [40], which uses a mixture of first and second derivative methods to minimize the error between actual and reconstructed pixel values. Although the parametric model is used to reduce the dimension of spectral sensitivity, the accuracy and efficiency is not compared to our proposed method.

Regarding the analysis of natural spectra, a number of studies have been investigated. Judd et al. [25] and Slater et al. [26] have analyzed the basis functions of outdoor illumination spectra; both of them concluded that the first three bases dominantly covers the entire spectral distributions. Grossberg [53] analyze the properties of camera response function. They collected a diverse database of real-world camera response functions (*DoRF*), and show the real-world responses occupy a small part of the theoretical space of all possible responses. A low-parameter empirical model of response (*EMoR*) is created from the combination of theoretical space and data from *DoRF*. Then the complete response function of a camera is accurately interpolated from a small number of measurements obtained using a standard chart. Several researchers have analyzed the reflectance of Munsell color chips and extracted the first four to eight basis functions [27] [28].

3.2 Spectral Sensitivity Estimation by Using Basis Functions

Basis functions reduces the dimension of spectral sensitivity, because the number of basis functions required are much less than the dimension of sensitivity itself. This reduces the number of unknowns in estimating sensitivity, and thus it provides more accurate results.

3.2.1 Image Formation

The image intensity is related to the incoming spectrum and the spectral sensitivity of a camera [46] [32]. Concretely, it can be described as

$$I_c = \int L(\lambda) q_c(\lambda) d\lambda, \tag{3.1}$$

where $L(\lambda)$ is the incoming spectrum, $q_c(\lambda)$ and I_c are the spectral sensitivity and the image intensity for R, G and B channels. The index c stands for R, G and B. The integration is calculated over the visible spectrum. This model has been verified as being adequate for computer vision over a wide variety of systems [23] [33] [32]. This model is also assumed for the human visual system and forms the basis for the CIE colorimetry standard after processing gamma function.

If we discretize Equation (3.1), then it becomes

$$I_c = \sum_{\lambda=1}^{W} L_\lambda q_{c\lambda}. \tag{3.2}$$

where λ is the index, W is the total number of elements, L_λ and $q_{c\lambda}$ are sampled values of $L(\lambda)/d\lambda$ and $q_c(\lambda)$, and $d\lambda$ is the sampling interval.

3.2.2 Recovering Spectral Sensitivity

If we use a vector notation to Equation (3.2), it can be converted to

$$I_c = [L_1, \cdots, L_W][q_{c1}, \cdots, q_{cW}]^t. \tag{3.3}$$

Let us suppose that we have a set of incoming spectra and corresponding image intensities. Then, Equation (3.3) becomes as follows by using a matrix notation:

$$\mathbf{I} = \mathbf{LQ} \tag{3.4}$$

where $\mathbf{I}$ is an $N \times 1$ matrix of image intensities (N is the number of different images), $\mathbf{L}$ is an $N \times W$ matrix of spectra (W is the number of samplings), and $\mathbf{Q}$ is an $W \times 1$ matrix of spectral sensitivity.

When $\mathbf{I}$ and $\mathbf{L}$ are known, $\mathbf{Q}$ can be solved as follows:

$$\mathbf{Q} = \mathbf{L}^{+}\mathbf{I} \tag{3.5}$$

where $\mathbf{L}^{+}$ is the psuedo inverse of $\mathbf{L}$ and is equal to $(\mathbf{L}^{t}\mathbf{L})^{-1}\mathbf{L}^{t}$.

Here, the size of the matrix $\mathbf{L}^{t}\mathbf{L}$ is $W \times W$. In order to calculate the inverse matrix of $\mathbf{L}^{t}\mathbf{L}$ robustly, its rank should be W. However, the rank of $\mathbf{L}$ is at most N when N is smaller than W. This happens when the number of samplings is more than the number of images. Then, the calculation of the inverse matrix becomes unstable because of rank deficient of matrix L. Consequently, basis functions are used to reduce the dimensions of spectra. Then, the spectral sensitivity becomes robust.

3.2.3 Benefits of Using Basis Functions

Spectral sensitivity can be robustly estimated from Equation (3.4) by using the basis functions of spectral sensitivity owing to its low dimensionality. Let us assume that the spectral sensitivity can be approximated by a linear combination of a small number of basis functions:

$$q(\lambda) = \sum_{i=1}^{D} q_i Q_i(\lambda) \tag{3.6}$$

where D is the number of basis functions, q_i is the coefficient and $Q_i(\lambda)$ is the basis function.

By substituting the equation into Equation (3.1), we can derive

$$\begin{aligned} R &= \int L(\lambda) \sum_{i=1}^{D} (q_i Q_i(\lambda)) d\lambda \\ &= \sum_{i=1}^{D} q_i \sum_{\lambda=1}^{W} L(\lambda) Q_i(\lambda) \end{aligned} \tag{3.7}$$

where R is the image intensity for the red channel, and image intensity for green and blue channels are calculated in the same way.

If we use another notation E_i to describe the multiplication of spectrum data and basis function of spectral sensitivity, namely,

$$E_i = \sum_{\lambda=1}^{W} L(\lambda) Q_i(\lambda), \tag{3.8}$$

then by substituting Equation (3.8) into (3.7), we obtain

$$R = \sum_{i=1}^{D} q_i E_i. \tag{3.9}$$

The same equations for blue and green channels can be obtained in the same manner.

Now, let us suppose that we have N set of data (image intensities and spectra). By using the matrix notation, we can describe Equation (3.9) as

$$\mathbf{I} = \mathbf{E}\mathbf{q}, \tag{3.10}$$

where I is the $N \times 1$ matrix, E is the $N \times D$ matrix, and $\mathbf{q}$ is the $D \times 1$ coefficient matrix. Consequently, this coefficient matrix $\mathbf{q}$ can be expressed as

$$\mathbf{q} = \mathbf{E}^{+}\mathbf{I} \tag{3.11}$$

where $\mathbf{E}^{+}$ is the pseudo inverse of the matrix $\mathbf{E}$.

If the rank of the matrix $\mathbf{E}$ is bigger than D, namely, if the number of images N is bigger than the number of dimension D, we can robustly estimate a unique solution of coefficient matrix $\mathbf{q}$. Then, we can correctly recover the spectral sensitivity.

3.3 Optimum Basis Functions

In order to find the optimum basis functions, we tried four different kinds of basis functions to describe the spectral sensitivity, which includes polynomials basis functions, Fourier basis functions, radial basis functions (RBF), and basis functions extracted by singular value decomposition (SVD).

3.3.1 Polynomial Basis Functions

Polynomial basis function is expressed as:

$$F = \sum_{i=0}^{D} a_i \lambda^i \tag{3.12}$$

where a_i is the coefficient. Using this polynomial basis functions, the spectral sensitivity is describe as a linear combination of λ^i (the value of i is from 0 to D) as shown in Equation (3.8). The Figure 3.1 shows the polynomial basis functions. In Figure 3.1, eight basis functions are shown with different colors.

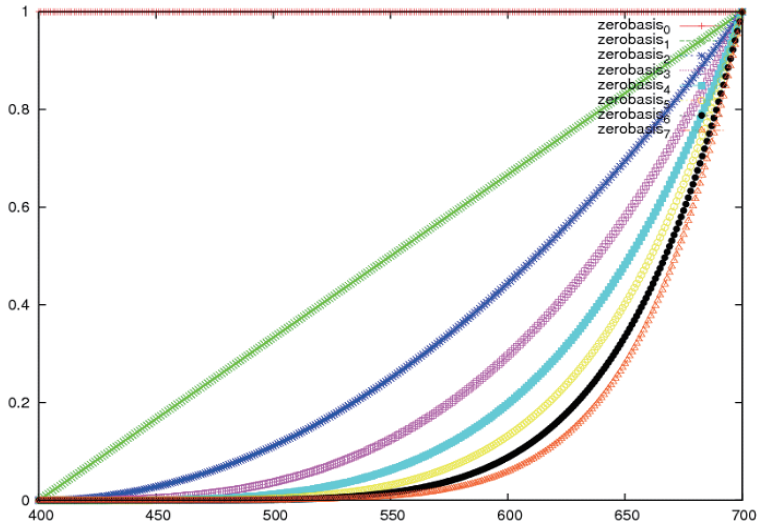

Figure 3.1: Polynomial basis functions.

3.3.2 Fourier Basis Functions

The basis functions of Fourier series is described as:

$$F = \sum_{i=0}^{D} a_i sin(i\lambda\pi) \tag{3.13}$$

where a_i is the coefficient. The Figure 3.2 shows the first four Fourier basis functions, the Figure 3.3 shows the other four Fourier basis functions.

3.3.3 Radial Basis Functions

By using Radial basis functions, the spectral sensitivity is represented as a sum of D radial basis functions, each associated with a different center μ, and weighted by an appropriate coefficient σ. The radial basis functions is written as:

$$F = \sum_{i=0}^{D} a_i \exp(-\frac{(\lambda - \mu_i)^2}{\sigma^2}) \tag{3.14}$$

The Figures 3.4, 3.5, 3.6 show the radial basis functions for R, G, and B channels, respectively.

The advantage of using the radial basis function is that these basis functions are similar to Gaussian function, also similar to the shape of spectral sensitivity. Hence, better results can be obtained by using the radial basis function.

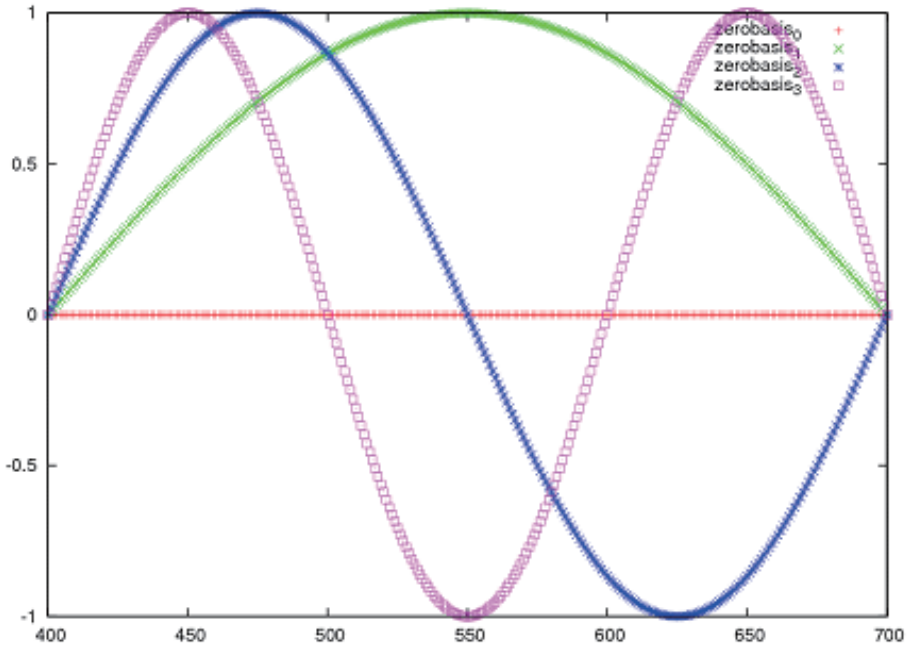

Figure 3.2: The first four Fourier basis functions.

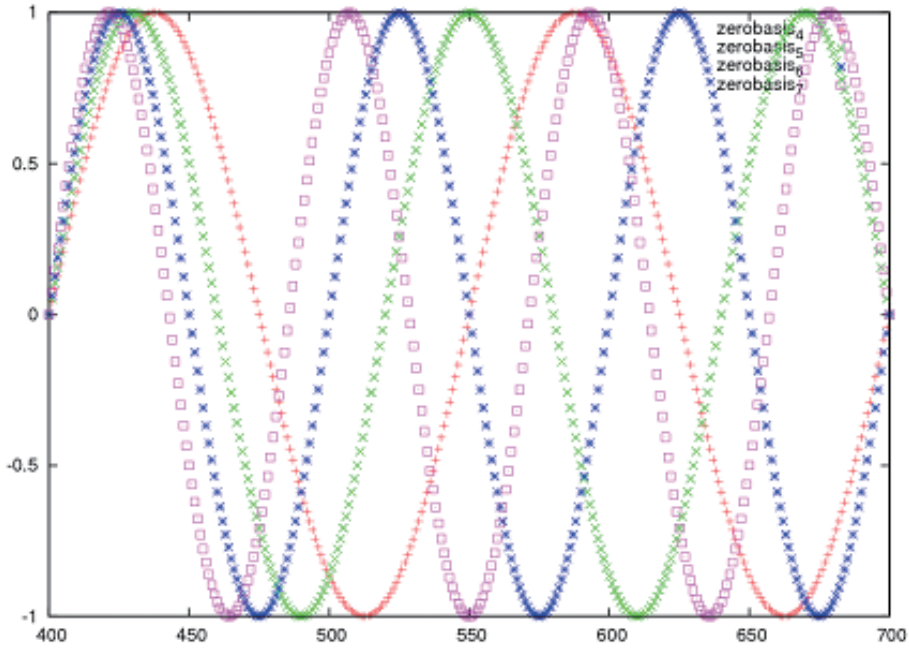

Figure 3.3: The Last four Fourier basis functions.

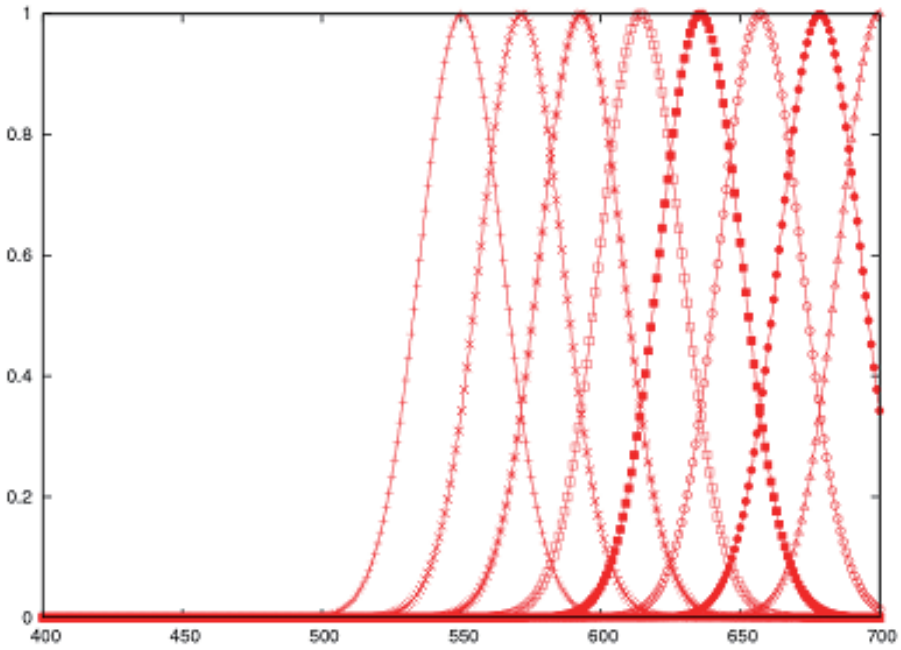

Figure 3.4: Red channel of radial basis functions.

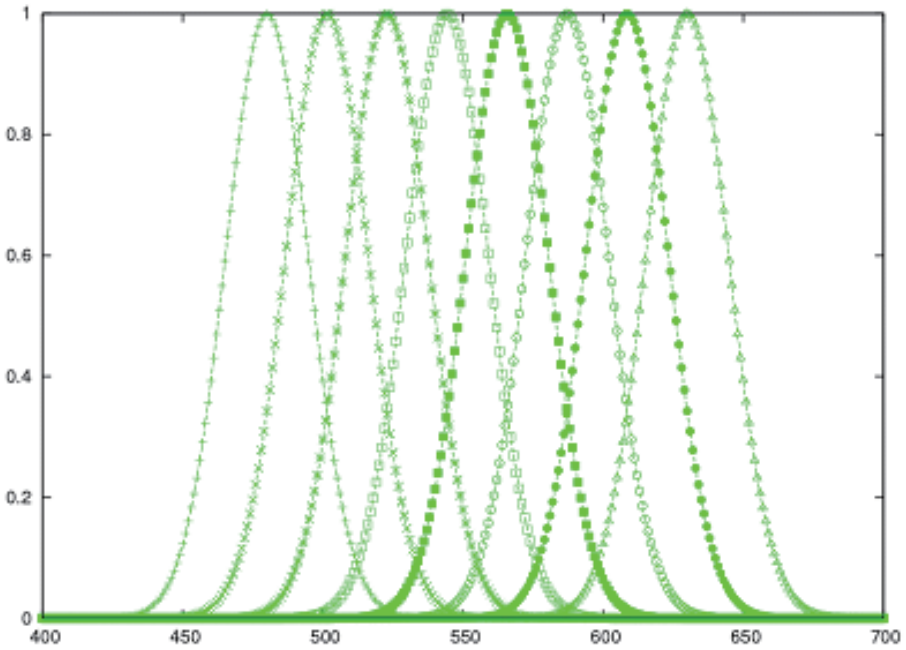

Figure 3.5: Green channel of radial basis functions.

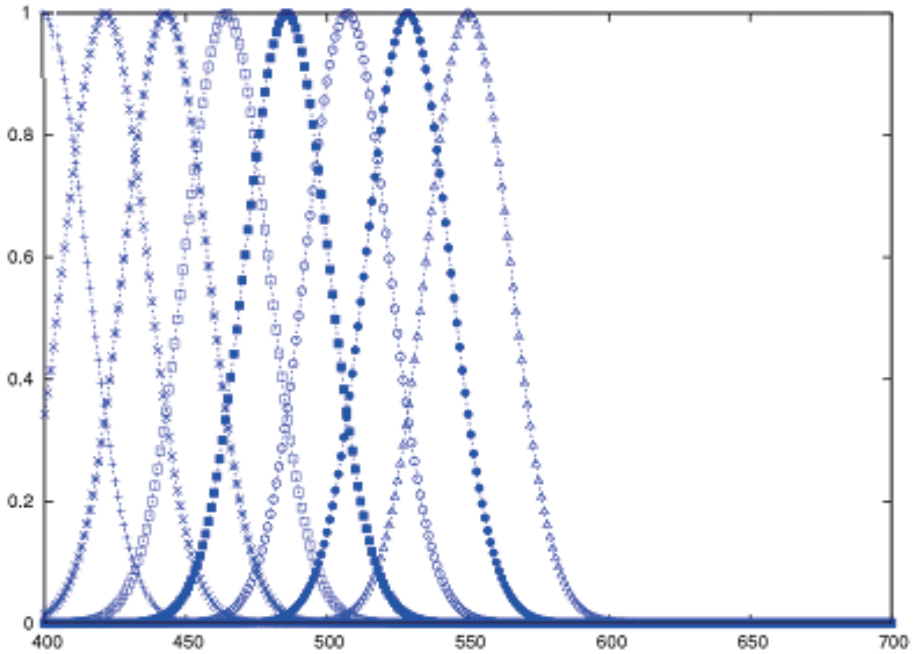

Figure 3.6: Blue channel of radial basis functions.

3.3.4 Basis Functions from Singular Value Decomposition

We collected several cameras and measured the spectral sensitivity for these digital cameras. Also we collected a few estimated spectral sensitivity from the literature. Then we made a database of spectral sensitivity.

By applying the singular value decomposition (SVD) for the database, we can calculate the eigenvectors and use these eigenvectors as the basis functions to estimate the spectral sensitivity of an arbitrary camera. Details of obtaining the sensitivity database and estimating the basis functions from the database are explained in the next section.

3.4 Experiment

This section shows the results of estimated spectral sensitivities by using four basis functions described in the previous section. By comparing the results obtained with different basis functions, we find the optimum set of basis functions which has the least error to estimate the spectral sensitivity for an arbitrary camera.

3.4.1 Obtaining Sensitivity Database

In the following experiment, we use the white board illuminated by the monochrometer, which could produce narrow-band illumination. While changing the wavelength, the image intensities and spectra of the white board are simultaneously captured by cameras and a spectrometer respectively. The spectral sensitivity is expressed as:

$$S(\lambda) = \frac{I(\lambda)}{n \cdot \int L(\lambda) d\lambda} \tag{3.15}$$

where $S(\lambda)$ is the spectral sensitivity, $I(\lambda)$ is the image intensity, $L(\lambda)$ is the spectrum, and n is a factor related to the camera aperture (F number), the exposure time and the electronic amplification (the ISO number).

For red channel of spectral sensitivity, we write the equation as shown in Equation (3.16), where N denotes the number of images taken by a camera and n_N denotes the combination of aperture, exposure time and amplification for the Nth image. The equations for blue and green channels can be obtained in the same way. Image intensity is read from captured image, and spectrum data are measured by a spectrometer. Thus, the spectral sensitivity is calculated from the above equation.

$$\begin{bmatrix} I_{R1} \\ I_{R2} \\ \vdots \\ I_{RN} \end{bmatrix} = \begin{bmatrix} n_1 \cdot L_1 \cdot S_{R1} \\ n_2 \cdot L_2 \cdot S_{R2} \\ \vdots \\ n_N \cdot L_N \cdot S_{RN} \end{bmatrix} \tag{3.16}$$

Intensity Linearization Image intensity is not linearly related to scene radiance recorded at the camera sensor. The function relating scene radiance to image intensity is called as the camera response function. Therefore, before using the image intensity which is read from images to calculate the spectral sensitivity, we must do the liearization first. For estimating the response function of these cameras, we use the method proposed by Takamatsu et al. [22]. This method is based on probabilistic intensity similarity measure which is the likelihood of two intensity observations corresponding to the same scene radiance. It requires a few images of a static scene taken from the same viewing position with fixed camera parameters. We took a few images of a Macbeth color chart for collected cameras to estimate the response function. The estimated response function of blue channel for Canon EOS Kiss Digital X camera is shown in Figure 3.7. The solid curve in this figure is the estimated response function, while the dotted line is used to make a contrast. For estimating the response function

of cameras whose result estimated by Takamatsu's method is not accurate, we changed the shutter speed of these cameras to capture images of a Macbeth color chart to do the estimation.

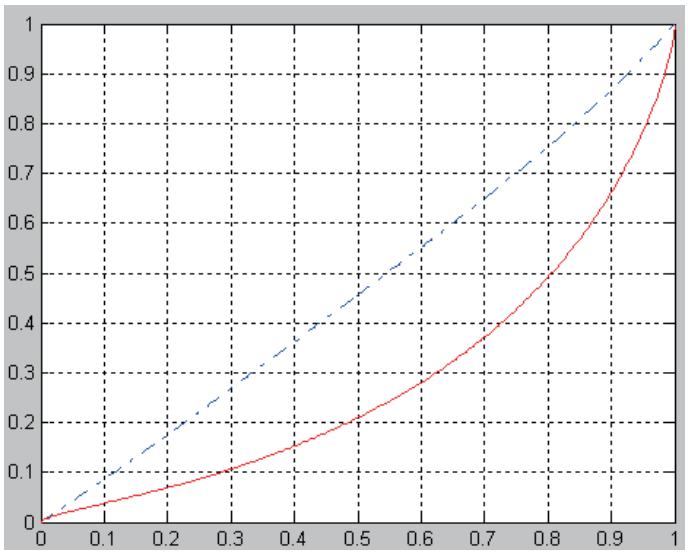

Figure 3.7: Estimated response function of blue channel for Canon EOS Kiss Digital X camera by Takamatsu's method.

Intensity Normalization When taking the images of a white board, according to different wavelength of the light spectrum, the camera parameters (n in Equation (3.15)) are changed. In order to calculate the spectral sensitivity using Equation (3.16), the image intensity have to be normalized. The normalization factor n in Equation (3.15) is expressed as:

$$n = \frac{ISO \cdot t}{F^2} \tag{3.17}$$

where ISO is the value of electronic amplification, t stands for the exposure time, and F means the f number of each image.

Spectrum Measurement The spectrum data of the white board are measured by a spectrometer, Photo Research PR-655 as shown in Figure 3.8. The spectrometer could measure the spectra from 380-780 nm at 4 nm increments.

Estimated Spectral Sensitivity We collected a few cameras, and estimated the spectral sensitivity by using Equation (3.16). In order to verify the accuracy of estimated spectral

Figure 3.8: Photo research PR-655 spectrometer [47].

sensitivity, we compared the error between the predicted image intensity and image intensity read from images. With the spectra measured by spectrometer and estimated spectral sensitivity, the predicted image intensity is calculated by using Equation (3.1). Macbeth color chart is used for this verification. Images of the first 18 patches (color patches) are used. The plotted data is shown in Figure 3.9. In this figure, the horizontal axes displays the predicted *RGB* values normalized by the maximum, while the vertical axes represents *RGB* values read from color chart patches. The data for *R*, *G*, and *B* channels are shown in different colors. Obviously, we could see from this figure that the predicted image intensity matches the real intensity very well. This proves that the spectral sensitivity measurement is quite accurate.

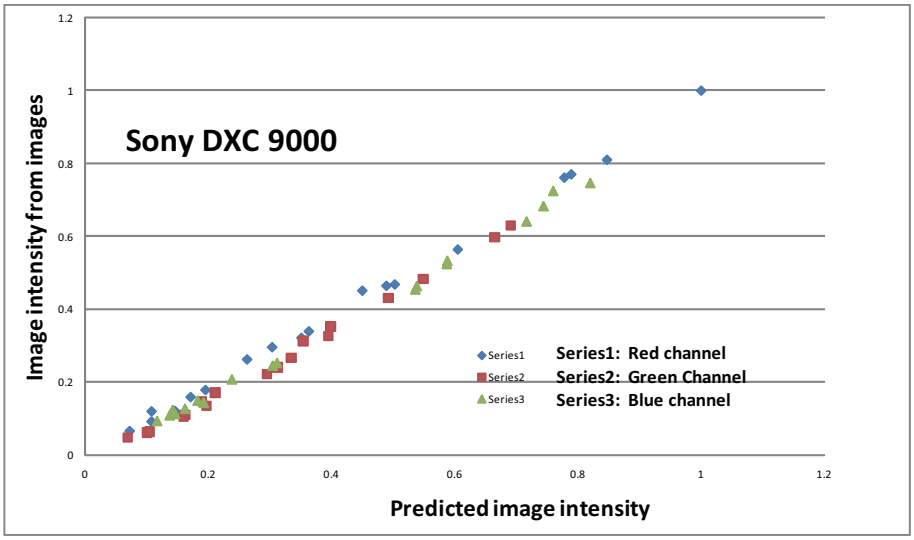

Figure 3.9: Accuracy verification of estimated spectral sensitivity of SONY DXC 9000.

Several results of spectral sensitivity are also obtained from the literature. All

the spectral sensitivity data are added into a database, then we apply the singular value decomposition (SVD) method for the database to extract the basis functions. The spectral sensitivity of SONY DXC 9000, Nikon D70 and Canon 10D are shown in Figures 3.10 and 3.11. The spectral sensitivity of SONY DXC 9000 is obtained by ourselves, and the measured spectral sensitivity is used as the ground truth for the evaluation experiment. The spectral sensitivity of Nikon D70 and Canon 10D are collected from the literature.

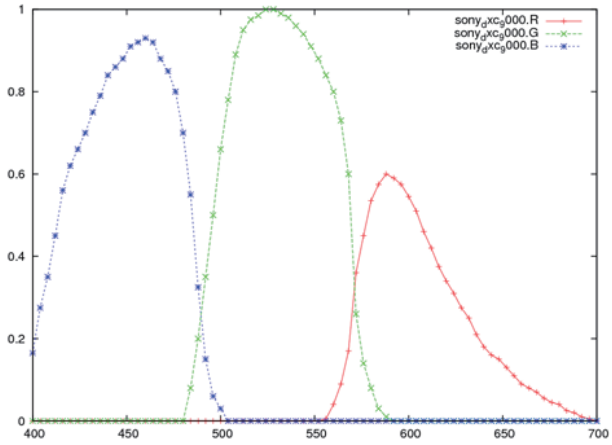

Figure 3.10: Spectral sensitivity of SONY DXC 9000.

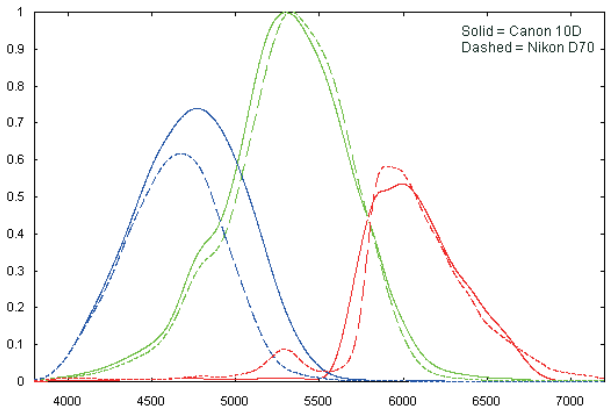

Figure 3.11: Spectral sensitivity of Nikon D70 and Canon 10D.

Extracted basis functions from sensitivity database From the database of spectral sensitivity, we compute the eigenvalues by SVD. The result of red channel is shown in Table 3.1.

Table 3.1: Percentage of each eigenvalue for red channel.

EigenValues	Percentage
5.574994	76.3%
0.788019	10.8%
0.428096	5.9%
0.261325	3.6%
0.137284	1.9%
0.115380	1.6%

From this table we see that for the first four eigenvalues the sum of their percentage is 97%. This means that we can take the corresponding eigenvectors to cover 97% information of spectral sensitivity.

Based on the analysis of eigenvalues, the number of basis functions can be decided. Then we obtain basis functions by extracting the eigenvectors of the spectral sensitivity database. The result is shown in Figure 3.12. The horizontal axes in this figure shows the wavelength, while the vertical axes represents the corresponding spectral sensitivity.

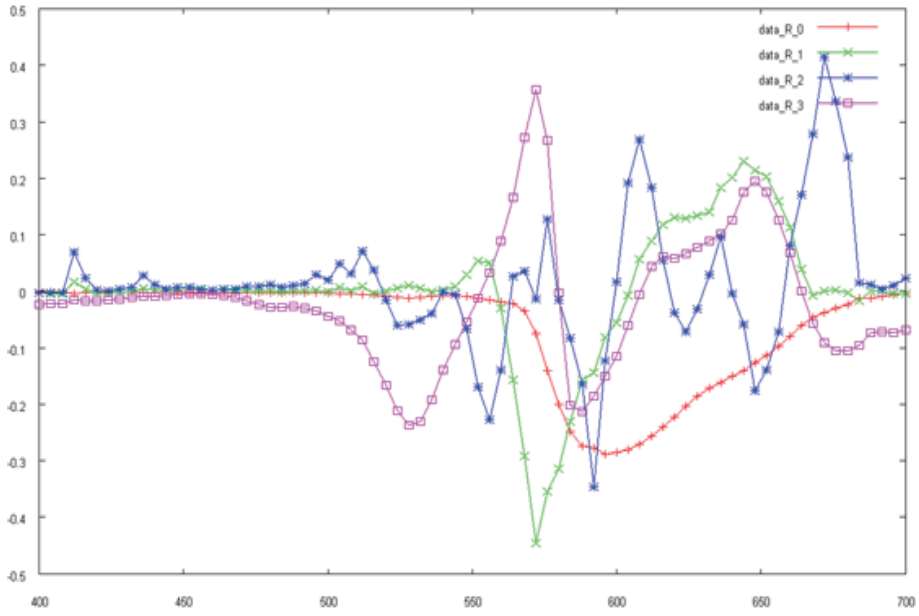

Figure 3.12: Extracted basis function of red channel by SVD.

These Figures 3.12, 3.13, and 3.14 show the *R*, *G*, and *B* channel of estimated basis functions by SVD from the spectral sensitivity database respectively. Not all the basis

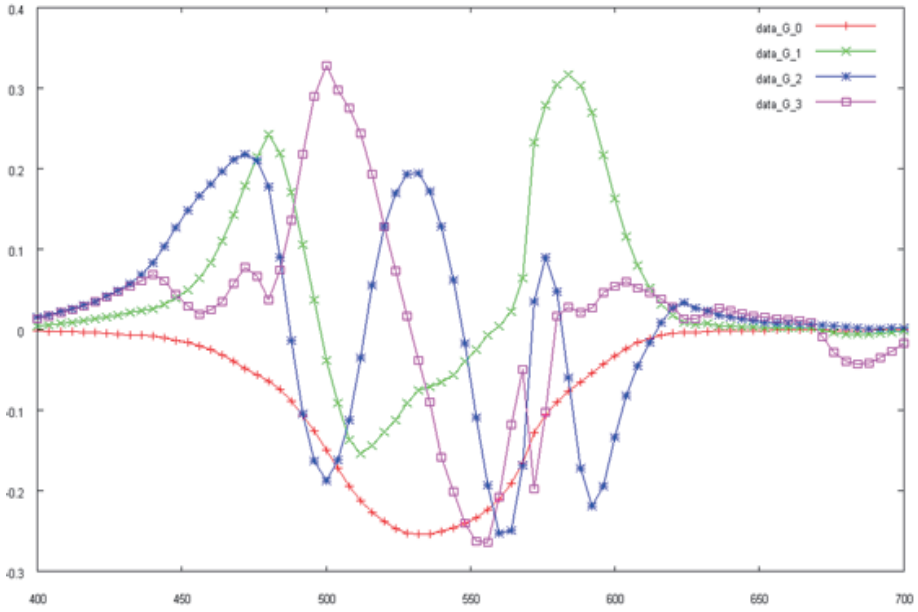

Figure 3.13: Extracted basis function of green channel by SVD.

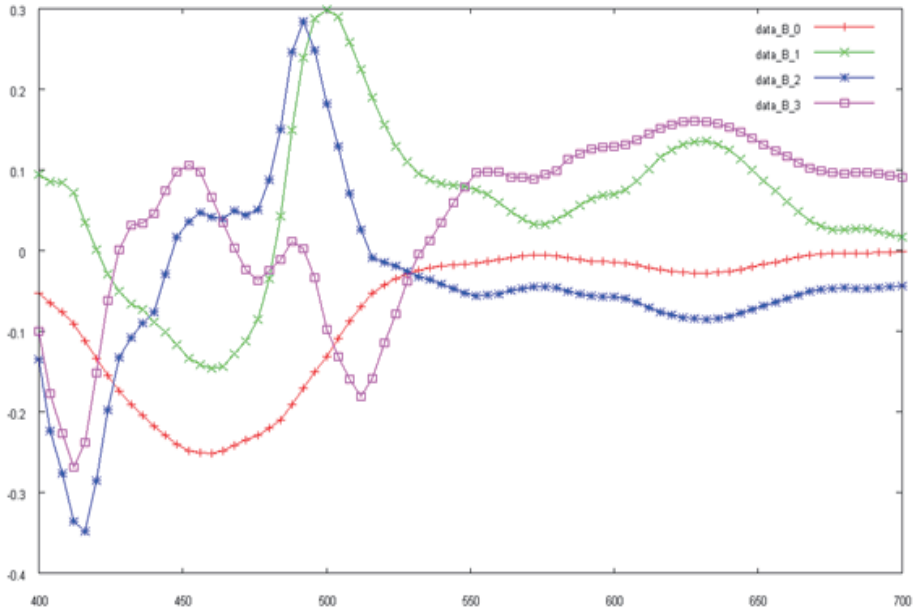

Figure 3.14: Extracted basis function of blue channel by SVD.

functions are shown here.

3.4.2 Evaluation of Optimum Basis Functions

As shown in Equation (3.11), the coefficient matrix is calculated from image intensity and multiplication of spectrum data and basis functions. Then we estimate the spectral sensitivity by multiplying the coefficient by corresponding basis functions. In order to evaluate the optimum basis functions which has least error, we did the experiment with a Macbeth color chart. The first 18 color patches are used. Image intensity and spectra are simultaneously captured by camera and spectrometer for each patch. Then, the linearized image intensity as shown in Figure 3.15 and spectra 3.16 and basis functions are used to estimate the camera sensitivity. The result of different basis functions are shown in Figures 3.17, 3.18, 3.19 and 3.20.

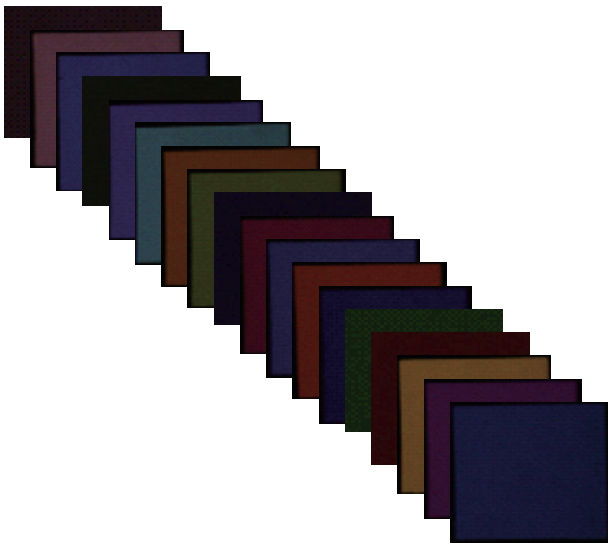

Figure 3.15: The first 18 patches of Macbeth color chart used for evaluation.

From these results, we see that the estimated spectral sensitivity from the extracted basis functions is the best, and that of polynomial bases is the worst, as expected. The radial basis functions may not be sufficiently accurate for estimating the spectral sensitivity, because the spectral sensitivity is not the complete Gaussian function. There are also some errors remained in the estimated spectral sensitivity from extracted basis functions by SVD. We think this as the error of response function, measured spectral sensitivity and image noises.

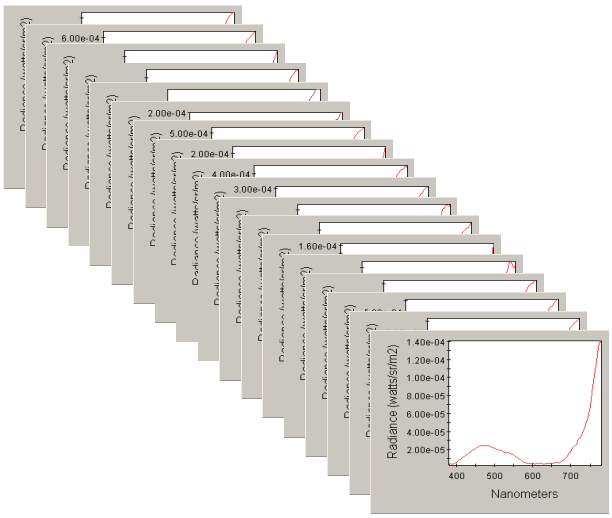

Figure 3.16: Captured spectra of each patch for evaluation by spectrometer.

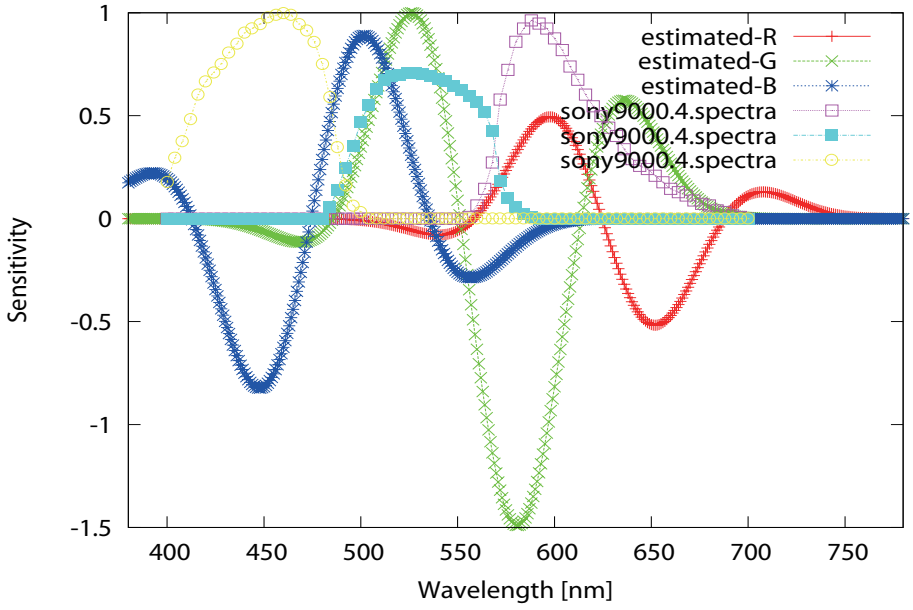

Figure 3.17: Spectral sensitivity estimated from Polynomial Basis Functions.

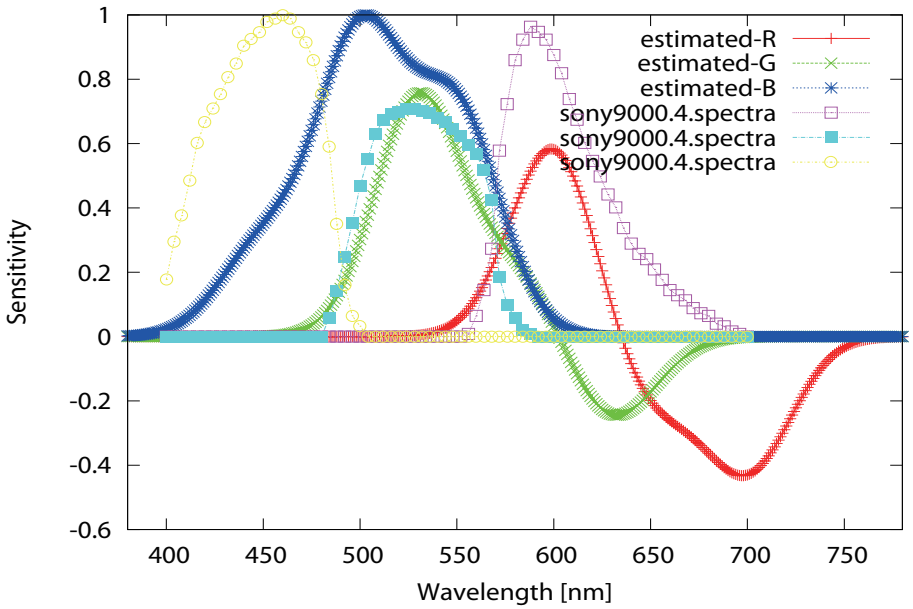

Figure 3.18: Spectral sensitivity estimated from Fourier Basis Functions.

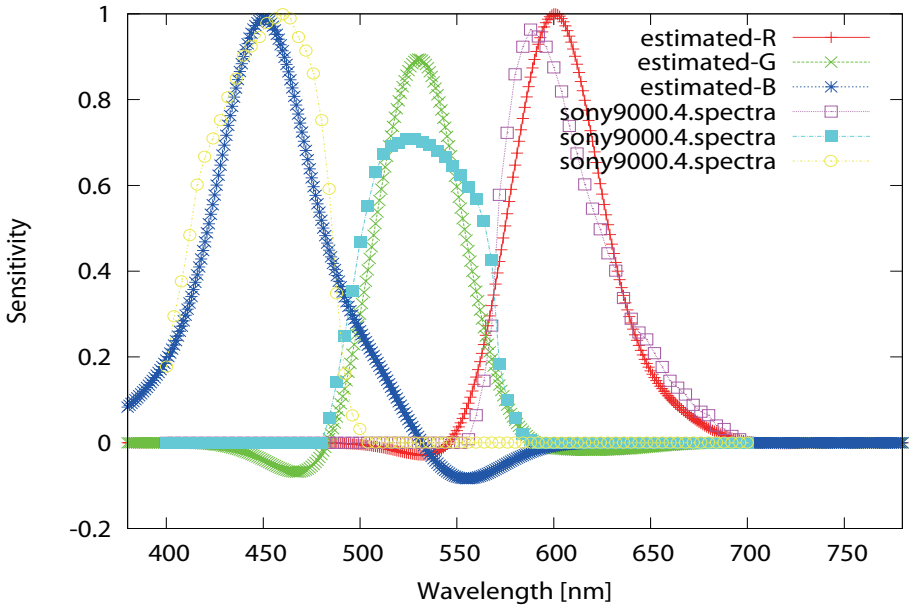

Figure 3.19: Spectral sensitivity estimated from Radial Basis Functions.

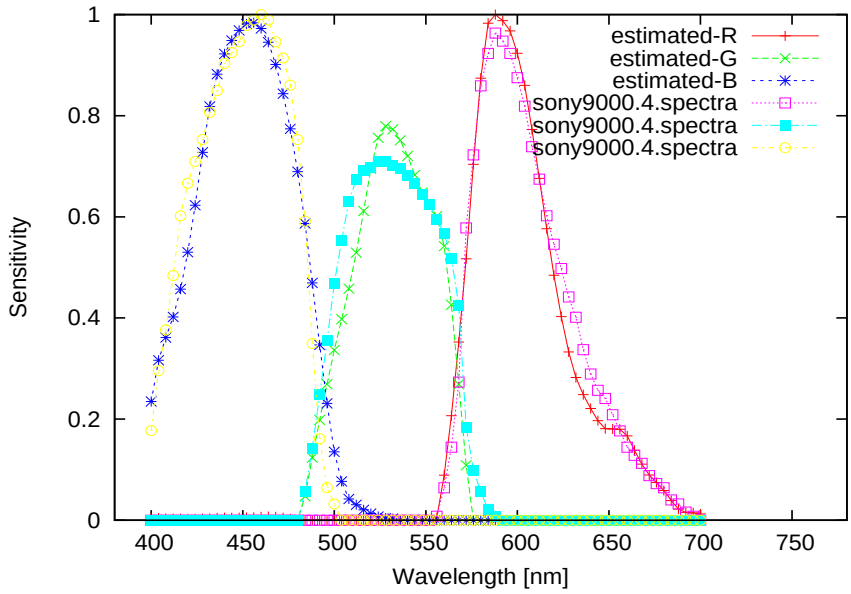

Figure 3.20: Spectral sensitivity estimated from Singular Value Decomposition (SVD).

3.5 Summary

In this chapter, we have analyzed the characteristic of spectral sensitivity and proposed a robust method to estimate the spectral sensitivity of digital cameras by using basis functions. We obtained the spectral sensitivity by measuring the collected digital cameras and from the literature. Then we added all these spectral sensitivity of different digital cameras to a database and extracted the basis functions by using the singular value decomposition (SVD). We compared the extracted basis functions by SVD with another three basis functions, polynomial basis functions and Fourier series and radial basis functions (RBF), to get the optimum set basis for spectral sensitivity estimation. Based on the experiment, we found that the extracted basis functions by SVD are much more suitable for estimating the spectral sensitivity of digital cameras.

Chapter 4

Conclusions

4.1 Summary

Physics-based vision is concerned with the physical relationship between an imaging sensor and the external world. The physical phenomenon that mediates this relationship is light. Consequently, two key components of physics-based vision are reflection model and sensor model. This thesis investigates these two key components, the reflection model and sensor model, and propose one novel method for each model. Specifically, for reflection model we proposed a practical method for estimating the reflectance properties of an outdoor diffuse object with the presence of inter-reflection. For sensor model, we proposed a reliable method for estimating the spectral sensitivity of arbitrary digital camera by using basis functions extracted from the database.

4.1.1 Reflectance Estimation with the Presence of Inter-reflection

To create a realistic model of a real world object by computer vision and graphics techniques has attracted interest from a wide range of research fields and industries in recent years. Shape and reflectance properties of the object are necessary to simulate the accurate appearance of an object. Obtaining the reflectance properties of an object remains a challenge, because it is usually very complicated especially for the concave object which has strong inter-reflection. We proposed a novel method to estimate the reflectance properties of an outdoor diffuse object with the presence of inter-reflection by assuming the object surface consists of hundreds of small facets. Then, the inter-

reflection effect on one facet is calculated as the incoming energy from all the other facets. Also, the occlusion problem between two facets has been solved perfectly. The occlusion affect the estimated reflectance so much that it makes the synthesized image very dark. For experiment results, the error between the synthesized image which is acquired by re-rending the object with estimated reflectance and captured radiance image is less than three percent, while the error of previous method [45] which does not take the inter-reflection into account is as big as sixty percent. This fact proves the proposed method for reflectance estimation with the presence of inter-reflection quite accurate.

4.1.2 Camera Sensitivity Recovery

Spectral sensitivity of digital cameras is non-trivial information for many computer vision and applications. Different cameras usually produce differently-colored images for the same scene due to the difference in the spectral sensitivity. Color of one camera can be converted into that of the other after acquiring the spectral sensitivity. Several methods of physics-based vision require spectral sensitivity, such as demosaicing, color correction and illuminant estimation algorithms. We investigate the characteristics of spectral sensitivities of digital cameras and propose a method to estimate the spectral sensitivity by using basis functions. We measured the spectral sensitivity of cameras and also collected data from the literature. Then, the basis functions are extracted from these collected data by singular value decomposition (SVD). In order to find the optimum set to estimate the spectral sensitivity, the extracted basis functions are compared with another three mathematical basis functions, the polynomial basis functions, the Fourier basis functions and the radial basis functions (RBF). The experiment result of estimated spectral sensitivity by using extracted basis functions has the least error. Consequently, we think the extracted basis functions from the database is reliable and adequate for spectral sensitivity estimation.

4.2 Contribution

In this thesis, we have investigated two key components of physics-based vision: the reflectance model and the sensor model. Specifically, we proposed a practical method to estimate the reflectance properties of outdoor diffuse object with the presence of inter-reflection for the reflectance model. For sensor model, we proposed a reliable

method to estimate the spectral sensitivity of digital cameras by using basis functions. The main contributions are summarized as follows:

Reflectance estimation with the presence of inter-reflection The main contribution of this work is the accurate inter-reflection estimation. The problem is solved by assuming the object surface consists of hundreds of small facets. The inter-reflection effect on one facet is calculated as the incoming light energy from all the other facets. The problem caused by occlusion between two facets is also solved by detecting whether the vector between two facets intersects with another facet or not. If intersection exists, no inter-reflection between these two facets is calculated.

Camera sensitivity recovery To estimate the spectral sensitivity robustly still remains a challenge, because of the high dimensionality of spectral sensitivity. Vora [32] measured the spectral sensitivity by using the monochromter. The estimated result is accurate, but the equipment is expensive and not readily available. Sharma [33] [34] improved the estimated spectral sensitivity by introducing various constraints, however the calculation is complicated. Thomson [38] proposed a method to estimate the spectral sensitivity by using a parametric model, but this method is not as accurate as ours. The main contribution is to estimate the spectral sensitivity by using basis functions, which are extracted from the database of measured spectral sensitivity of different digital cameras. Consequently, the algorithm becomes robust and efficient. None of the method introduced above is as simple and efficient and robust as ours.

4.3 Future Work

These two proposed methods for estimating the reflectance properties with the presence of inter-reflection and camera sensitivity recovery made significant progress. However, there are still some issues remained.

Internet color constancy With the recent rise in popularity of Internet photo sharing sites like Flickr and Google, community photo collections (CPCs) have emerged as a powerful new type of image dataset. This kind of data presents a singular opportunity: to estimate the shape and optical information and make a 3D model automatically. For estimating the shape information from this dataset, the big problem is the tremendous variation in viewing parameters. While traditional multi-view stereo algorithms have

considered images with far less appearance variation, where computing correspondence is significant easier, and have operated on somewhat regular distributions of viewpoints, the structure from motion method could be used to handle this problem. For acquiring the optical information, the big problem is the tremendous variation in appearance. These images are acquired by an assortment of cameras at different times of day and in various weathers. The possible solution of estimating the optical information is color constancy method. The spectral sensitivity is an essential factor for most color constancy algorithms.

Chapter 3 explains the proposed method of estimating the spectral sensitivity of digital cameras by using basis functions. By using the basis functions, the dimensionality of spectral sensitivity is reduced, hence the estimation becomes robust. However, spectra in the experiment is measured by the spectrometer, this equipment is not available for the CPCs. Hence, next we plan to estimate both spectra and spectral sensitivity from image dataset available on the internet. After the spectral sensitivities of cameras are known, the images captured by one camera can be converted into images captured by the other. Then, the color constancy method will be used to estimate the object surface color without the influence of illumination. Combined with the shape information acquired by structure from motion method, we manage to automatically estimate the shape and optical information from the dataset to make a realistic three dimensional model.

References

[1] K. Ikeuchi, and D. Miyazaki,"Digitally Archiving Cultural Objects." *Springer science Business Media,* LLC, 2008.

[2] K. Ikeuchi, T. Oishi, J. Takamatsu, R. Sagawa, A. Nakazawa, R. Kurazume, K. Nishino, M. Kamakura and Y. Okamoto, "The great buddha project: Digitally archiving, restoring, and analyzing cultural heritage objects." *In1 J. Com. V. 75-1,* pp.189-208, 2007.

[3] S. K. Nayar, K. Ikeuchi, and T. Kanade,"Shape from Interreflections." *International Journal of Computer Vision, 6: 3,* 173-195, 1991.

[4] Y. Yu, P. Debevec, J. Malik, and T. Hawkins,"Inverse Global Illumination: Recovering Reflectance Models of Real Scenes from photographs." *SIGGRAPH,* 1999.

[5] K. Pulli, M. Cohen, T. Duchamp, H. Hopper, L. Shapiro and W. Stuetzle, "View-based rendering: Visualizing real objects from scanned range and color data." *in Proc. EUROGRSPHICS Workshop,* pp.23-34, 1997.

[6] P. J. Neugebauer, and K. Klein, "Texturing 3D models of real world objects from multiple unregistrated photographic views." *Computer Graphics Forum,* pp.18-3, 245-256, 1999.

[7] H. P. A. Lensch, W. Heidrich, and H. P. Seidel, "Automated texture registration and stitching for real world models." *Pacific Graphics,* pp.317-326, 2000.

[8] L. Wang, S. B. Kang, R. Szeliski and H. Y. Shum,"Optimal texture map reconstruction from multiple views." *in Proc. CVRP,* pp.347-354, 2001.

[9] F. Bernardini, I. M. Martin, and H. Rushmeier,"High quality texture reconstruction from multiple scans." *IEEE Trans. Vis. Comput. Graph. 7-4,* pp.318-332, 2001.

[10] K. J. Dana, B. van Ginekken, S. K. Nayar, and J. J. Koenderink,"Reflectance and texture of real-world surfaces." *CVPR,* pp.151-157, 1999.

[11] S. Lin and S. W. Lee,“Estimation of diffuse and specular appearance.” *in Proc. ICCV,* pp.855-860, 1999.

[12] T. Machida, N. Yokoya and H. Takemura,“Surface reflectance modeling of real objects with interreflections.” *in Proc. ICCV,* pp.170-177, 2003.

[13] I. sato, T. Okabe, Y. sato and K. Ikeuchi,“Appearance sampling for obtaining a set of basis images for variable illumination.” *in Proc. ICCV,* pp.800-807, 2003.

[14] H. Winnemoller, A. Mohan, J. Tumblin, and B. Gooch,“Light waving: Estimating light positions from photographs alone.” *Computer Graphics Forum 24-3,* pp.433-438, 2005.

[15] Y. Sato, M. D. Wheeler, and K. Ikeuchi,“Object Shape and Reflectance Modeling from Observation.” *SIGGRAPH,* pp.379-387, 1997.

[16] S. K. Nayar, G. Krishnan, M. Grossberg, and R. Raskar,“Fast separation of Direct and Global Components of a Scene using High Frequency Illumination.” *SIGGRAPH,* pp.935-944, 2006.

[17] Y. Weiss,“Deriving intrinsic images from image sequences.” *ICCV,* pp.68-75, Volume 2, 2001.

[18] Brainard, D. H.,“Bayesian method for Reconstructing Color Images from Trichromatic Samples.” *IS&T, 47th Annual Conference,* pp.375-380, 1994.

[19] Vrhel, M. J., and Trussell, H. J.,“Filter Considerations in Color Correction.” *IEEE Transactions on Image Processing, Vol. 3, No. 2,* pp.147-161, 1994.

[20] Freeman, W. T. and Brainard, D. H.,“Bayesian decision theory, the maximum local mass estimate, and color constancy.” *Proceedings of the 5th International Conference on Computer Vision,* pp.210-217, 1995.

[21] Maloney, L. T. and Wandell, B. A.,“Color constancy: a method for recovering surface spectral reflectances.” *Journal of the Optical Society of America-A vol. 3,* pp.29-33, 1986.

[22] 高松淳，松下康之，池内克史，“輝度の確率的類似度によるカメラレスポンス関数の推定．” *in Proc. Meeting on Image Recognition and Uunderstanding,* (MIRU) 2008.

[23] P. L. Vora, J. E. Farrell, J. D. Tietz, D. H. Brainard, "Digital color cameras - 2 - spectral response." *HP Technical Report,* 1997.

[24] J. Y. Hardeberg, H. Brettel, F. Schmitt, "Spectral characterization of electronic cameras." *Electronic Imaging: Processing, Printing, and Publishing in Color,* Jan Bares; Ed. 1998.

[25] D. B. Judd, D. L. Macadam, G. Wyszecki, "Spectral distribution of typical daylight as a function of correlated color temperature." *J. Opt. Soc. Am.*, 54(8): 1031-1040, 1964.

[26] D. Slater, G. Healey, "What is the spectral dimensionality of illumination functions in outdoor scenes." *CVPR,* pp. 105-110, 1998.

[27] J. P. S. Parkkinen, J. Hallikainen, T. Jaaskelainen, "Characteristic spectra of Munsell colors." *J. Opt. Soc. Am. A,* 6(2):318-322, 1989.

[28] J. Cohen, "Dependency of the spectral reflectance curves of Munsell color chips." *Psychonomic. Sci.,* 1:369-370, 1964.

[29] Y. Matsushita, K. Nishino, K. Ikeuchi, M. Sakauchi, "Illumination normalization with time-dependent intrinsic images for video surveillance." *IEEE Transactions on Pattern Analysis and Machine Intelligence Vol.26,* No. 10, pp.1336-1347, 2004.

[30] Y. Yu, J. Malik, "Recovering photometric properties of architectual scenes from photographs." *In ACM Transactions on Graphics (Proceedings of ACM SIGGRAPH 1998),* pp.207-218, 1998.

[31] P. Debevec, C. Tchou, A. Gardner, T. Hawkins, C. Poullis, J. Stumpfel, A. Jones, N. Yun, P. Einarsson, T. Lundgren, M. Fajardo, P. Martinez, "Estimating surface reflectance properties of a complex scene under captured natural illumination." *USCICT Technical Report ICT-TR-06,* 2004.

[32] P. L. Vora, J. E. Farrell, J. D. Tietz, D. H. Brainard, "Digital color cameras - 2 - Spectral response." *Hewlett-Packard Laboratory Technical Report, Number HPL-97-54,* 1997.

[33] G. Sharma, H. J. Trussell,"Characterization of scanner sensitivity." *Proceedings of the IS&T and SID's Color Imaging Conference: Transforms & Transportability of Color. Springfield (VA): The Society for Imaging Science and Technology,* pp.103-107, 1993

[34] G. Sharma, H. J. Trussell,"Set theoretic estimation in color scanner characterization." *J Elec Imag, 5,* pp.479-489, 1996.

[35] P. M. Hubel, D. Sherman, J. E. Farrell,"A comparison of method of sensor spectral sensitivity estimation." *Proceedings of the IS&T/SID 2nd Color Imaging Conference: Color Science, Systems, and Applications. The Society for Imaging Science and Technology; Springfield (VA),* pp.45-48, 1994

[36] W. K. Pratt, C. E. Mancill,"Spectral estimation techniques for the spectral calibration of a color image scanner." *Appl Opt, 15,* pp.73-75, 1976.

[37] K. Barnard, B. Funt,"Camera characterization for color research." *Color: Research and applications, Vol. 27, No. 3,* 2002.

[38] M. Thomson, S. Westland,"Colour-imager characterization by parametric fitting of sensor responses." *Color: Research and applications, Vol. 26, No. 6,* pp.442-449, 2001.

[39] B. R. Frieden,"Probability, statistical optics and data testing." *Berlin: Springer-Verlag,* 1983.

[40] Marquardt, "Levenberg-Marquardt technique." *Society for Industrial and Applied Mathematics, 11,* pp.431-441, 1963.

[41] F. E. Nicodemus, J. C. Richmond, J. J. Hsia, I. W. Ginsberg, T. Limperis, "Geometrical considerations and nomenclature of reflections." *NBS Monograph 160, National Bureau of Standards, October,* 1977.

[42] *http://radsite.lbl.gov/radiance.*

[43] *http://www.meab-mx.se/tidning/cyrax2500.htm.*

[44] *Point Grey Research: http://www.ptgrey.com.*

[45] S. Okura, R. Kawakami, and K. Ikeuchi, "Efficient estimation of diffuse surface reflectance in an outdoor scene using spherical images." *MIRU,* 2008.

[46] B. K. P. Horn, "Robot Vision." *Cambridge (MA): MIT Press,* 1986

[47] Photo research PR-655 spectrometer *http://www.photoresearch.com/current/pr655.asp*

[48] D. H. Brainard and W. T. Freeman, "Bayesian color constancy." *JOSA,* 14(7):1393-1411, 1997.

[49] G. Finlayson, S. Hordley, and I. Tastl, "Gamut constrained illuminant estimation." *IJCV,* 67(1):93-109, 2006.

[50] G. D. Finalayson and S. D. Hordley and P. Hubel, "Color by correlation: a simple, unifying, framework for color constancy." *PAMI,* 23(11):1209-1221, 2001.

[51] A. Gijsenij and T. Gevers, "Color constancy using natural image statistics." *In Proc. CVPR,* pages 1-8, 2007.

[52] R. T. Tan, K. Nishino and K. Ikeuchi, "Color constancy through inverse intensity-chromaticity space." *JOSA,* 21(3):321-334, 2004.

[53] M. D. Grossberg and S. K. Nayar, "What is the space of camera response functions?" *IEEE Conference on Computer Vision and Pattern Recognition (CVPR),* Vol.2, pp.602-609, 2003.

[54] R. Y. Tsai, "An efficient and accurate camera calibration technique for 3d machine vision." *In Proceedings of 1986 IEEE Computer Society Conference on Computer Vision and Pattern Recognition (CVPR'86),* pp.364-374, 1986.

[55] S. Mann and R. Picard, "Being 'undigital' with digital cameras: Extending dynamic range by combining differently exposed pictures'." *In Proc. of IS&T 48th Annual Conf.,* pages 422-428, 1995.

[56] P. E. Debevec and J. Malik, "Recovering high dynamic range radiance maps from photographs." *In Proc. of ACM SIGGRAPH,* pages 369-378, 1997.

[57] R. Basri and D. Jacobs, "Photometric stereo with general unknown lighting." *In Proceeding of 2001 IEEE Computer Society Conference on Computer Vision and Pattern Recogition (CVPR'01),* pp.374-381, 2001.

[58] A. Hertzmann, S. M. Seitz, "Example-based photometric stereo: Shape reconstruction with general, varying brdfs." *IEEE Transaction on Pattern Analysis and Machine Intelligence,* Vol.27, pp.1254-1264, 2005.

[59] T. Chen, M. Goesele, H. P. Seidel, "Mesostructure from specularity." *In Proceedings of IEEE Computer Society Conference on Computer Vision and Pattern Recogition (CVPR'06),* Vol.2, pp.1825-1832, 2006.

[60] R. Cook and K. Torrance, "A reflectance model for computer graphics." *ACM Transactions on Graphics (Proceedings of ACM SIGGRAPH 81)*, pp.506-512, 1981.

[61] P. Debevec, T. Hawkins, C. Tchou, H. P. Duiker, W. Sarokin and M. Sagar, "Acquiring the reflectance field of a human face." *In Proceedings of the 27th annual conference on computer graphics and interactive techniques*, pp.145-156, 2000.